Effective Date: 07/05/2023
Expiration Date: 07/05/2028

XRISM/ Resolve
CMO
07/05/2023
RELEASED

INSTRUMENT CALIBRATION REPORT

RESOLVE TIMING COEFFICIENTS

RESOLVE-SCI-RPT-0065

REVISION (B)

XRISM-RESOLVE-CALDB-COEFTIME-207

X-ray Imaging and Spectroscopy Mission (XRISM) Project

NASA/GSFC Code 461

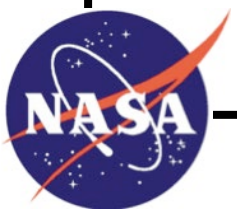

Check https://ipdtdms.gsfc.nasa.gov
to verify that this is the correct version prior to use

RESOLVE-SCI-RPT-0065
Revision B
Effective Date: 07/05/2023

Resolve Timing Coefficients

Signature/Approval Page

Prepared by: Makoto Sawada, Caroline Kilbourne, Tomoki Omama, Yuto Mochizuki, Masahiro Tsujimoto, and the Resolve Instrument Team

Reviewers/Approvers:

Megan Eckart
Maurice Leutenegger
Matthew Holland
Michael Lowenstein
Caroline Kilbourne
Tahir Yaqoob

Approved by:

Megan Eckart

***** Electronic signatures are available on-line at: https://ipdtdms.gsfc.nasa.gov*****

Preface

This document is an XRISM Project signature-controlled document. Changes to this document require prior approval of the applicable Product Design Lead (PDL) or designee. Proposed changes shall be submitted in the Technical Data Management System (TDMS) via a Signature Control Request (SCoRe) along with supportive material justifying the proposed change. Changes to this document will be made by complete revision.

All of the requirements in this document assume the use of the word "shall" unless otherwise stated.

Questions or comments concerning this document should be addressed to:
XRISM Configuration Management Office
Mail Stop: 461
Goddard Space Flight Center
Greenbelt, Maryland 20771

Change History Log

Revision	Effective Date	Description of Changes (Reference the SCoRe Approval Date)
(-)	11/08/2019	Released per RESOLVE-SCoRe-0317 First delivery. Values based on the Hitomi/SXS results.
(A)	04/07/2020	Minor updates. Nearly all of the values remain based on Hitomi/SXS results. Released per RESOLVE-SCoRe-0423
(B)	07/05/2023	The *Resolve* ground calibration results were incorporated, updating the SXS values updated for all parameters in ARRCOEFFS and the anti-co window parameters in DELTIMES. Release per RESOLVE-SCoRe-0555

NOTE to editors: The document name will be XRISM-CAL-RPT-XXXX, where XXXX is assigned by the TDMS system. The document will be cross-referenced in TDMS to the filename in the format XRISM-XXX-CALDB-FILEDESC-NN where XXX is the instrument or component (e.g. RESOLVE), FILEDESC refers to a specific calibration report (e.g., rmfparams) and NN the corresponding number assigned to that report by the SDC. For example the calibration report addressing the Resolve LSF calibration may be assigned XRISM-RESOLVE-CALDB-RMFPARAMS-01, that addressing the Resolve gain calibration XRISM-RESOLVE-GAINPIX-CALDB-02, etc. (where the numbers are to be provided by the SDC).

These documents are updated as needed, e.g. when the relevant CALDB files, or the relevant calibration data analysis, is revised. The document version will be assigned by the TDMS system. The tracking tool should be used to record changes.

This document must include the CalDB file name, an explanation of how the data were collected and the analysis conducted and, if using standard Ftools, the software version number. All revisions are consolidated into the same document to maintain a full record of all changes.

Table of Contents

1 Introduction

1.1 Purpose

This document describes the CALDB file containing parameters related to the timing of Resolve events. These parameters are divided into two categories: a set of timing coefficients which are used to convert trigger times recorded by the digital pulse processor to obtain photon arrival times; and a set of timing intervals used to assign event grades and coincidences. The timing coefficients are stored in the `ARRCOEFFS` extension, and the timing intervals are stored in the `DELTIMES` extension.

1.2 Scientific Impact

The two roles of the timing coefficients and timing intervals are to improve the relative timing and optimize time coincidence screening of the detector background events, with a minimal loss of events due to the false coincidence, and to adjust absolute timing so that temporal information extracted from the Resolve observations can be compared to results with other astrophysical observatories.

1.3 Formalization

In this section, the formalization of the timing coefficients and timing intervals, expected to be common to all CALDB releases, is described. If any updates are made in the formalization or in the CALDB format, then only the latest one is described here, and obsolete definitions will be moved to the Remarks section of each release.

Trigger times are assigned onboard by the Pulse Shape Processor (PSP). The PSP algorithm is unchanged from Hitomi/SXS, making the timing capability of Resolve identical to that of SXS. Therefore, the formalization of timing coefficients used for SXS [1] can be used for Resolve. Other timing parameters also use the same formalization as in SXS, since the timing behavior of the calorimeter pixels and anti-coincidence detector (hereafter, anti-co) are also unchanged from SXS. The only exceptions are minor changes in the CALDB file format, which are described in the Remarks section of the first delivery (Section 2.4).

ARRCOEFFS

The assignment of raw trigger times recorded by the PSP depends on event grade (Table 1). The first five grades (`TYPE`/`ITYPE` = Hp/0, Mp/1, Ms/2, Lp/3, and Ls/4) are triggered and properly telemetered events. These are subject to further data processing including time-coincidence screenings, and can be used for scientific analysis. Thus, their trigger times need to be converted

to calibrated, photon arrival times. This conversion is realized by timing coefficients stored in the ARRCOEFFS extension of this CALDB file. The other grades are for pseudo-events, for which triggering information does not exist (BL/5: random samples of baseline pulses while the PSP gets no triggers) or has been lost (EL/6; events lost due to buffer overflow, etc). Therefore, the "trigger times" for these grades have nothing to do with real event triggers, and do not need further calibration. Thus, there are no timing coefficients for these grades, and we do not discuss these any further in this report. Note that this follows time system conversion between the following: the PSP time counter, the Resolve local time, and the satellite time, as summarized in Table 2. The `rslsamcnt` task performs the conversion from the PSP time counter to the Resolve local time, as well as that from trigger times to photon arrival times. This is followed by the conversion from Resolve local time to satellite time by application of the `xatime` task. In this report, we focus on the conversion from trigger times to photon arrival times and do not strictly distinguish the three time systems, unless otherwise stated. See [2] and [3] for the details on these time systems.

Table 1 Summary of the definition of trigger times assigned by the PSP

Grade (TYPE/ITYPE)		Trigger time assigned by the PSP	Timing coefficients in ARRCOEFFS?
Hp	0	Initially at the time at which the pulse derivative exceeds the trigger threshold, which is then shifted by TICK_SHIFT.	Yes
Mp	1		Yes
Ms	2		Yes
Lp	3	At the time the pulse derivative is maximum (time of DERIV_MAX).	Yes
Ls	4		Yes
BL	5	Start time of the baseline sample record.	No
EL	6	Start time of the event lost duration.	No

Table 2 Summary of major time-related telemetry.

	PSP time counter	Resolve local time	Satellite time
Trigger time	TRIG_LP	SAMPLECNTTRIG	TRIGTIME
Photon arrival time	(N/A)	SAMPLECNT	TIME

For H-res and M-res events (TYPE=Hp, Mp, and Ms or ITYPE=0–2), trigger times are originally defined at which pulse derivative exceeds the trigger threshold (Figure 1, top). The original trigger times have a large energy dependence. For lower energy x-rays, the trigger threshold is higher in terms of the relative level to the peak of the derivative (DERIV_MAX). This makes the trigger time later relative to the true start of the pulse rise, compared to higher energy photons (Figure 1, middle). This effect can be corrected by adding a shift, called

TICK_SHIFT[1]. This is the time shift required to be added to the template to get the maximum of the pulse height calculated with the optimal filter (see [2] and [3] for the details). By adding the shift, it effectively aligns pulses near the time of DERIV_MAX (Figure 1, bottom). Note that the TICK_SHIFT correction is done onboard by updating TRIG_LP.

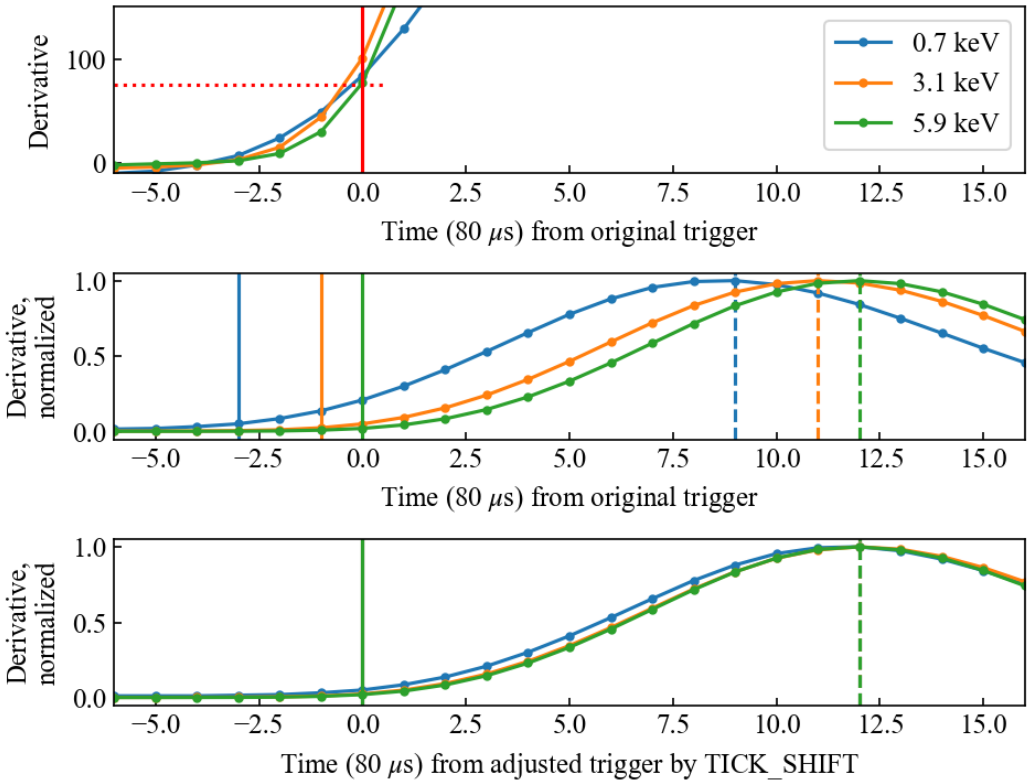

Figure 1 Example of pulse derivatives and corresponding trigger times for different energies, taken from Hitomi SXS in-orbit data. Top: Pulse derivatives near the trigger points, Middle: the same as the top panel, but with the amplitudes normalized, Bottom: the same as the middle panel, but with the time origin shifted from the original trigger by TICK_SHIFT. The red horizontal and vertical lines in the top panel show the trigger threshold (=75) and the original trigger point, respectively. The solid vertical lines in the lower two panels show the adjusted trigger points by TICK_SHIFT. The dashed vertical lines in the lower two panels show the times of DERIV_MAX.

On the other hand, for L-res events (TYPE=Lp and Ls or ITYPE=3–4), adjacent pulses are too close to each other to perform the optimal filtering. Therefore, the TICK_SHIFT correction is also not available. As mentioned above, the original trigger time without the TICK_SHIFT

[1] TICK_SHIFT is integer values in units of 80 μs. The finer-resolution component of the time shift obtained with the optimal filter is recorded as TIME_VERNIER with 5 μs resolution. Unlike TICK_SHIFT, the correction for TIME_VERNIER is not done onboard, but in the calculation of SAMPLECNTTRIG by rslsamcnt.

correction has a large energy dependence, and thus its use is not optimal. Instead, the time of DERIV_MAX is used, as it is less energy dependent (dashed lines in the bottom panel of Figure 1). However, as a side effect, this causes the L-res times to be systematically later than those of H-res and M-res events (solid lines in the same panel). To correct this requires that the conversion from trigger times to photon arrival times be grade dependent.

It is also possible that assigned trigger times are different from pixel to pixel, particularly for H and M-res events, as the trigger threshold and template used in the optimal filtering are defined for each pixel. Because the TICK_SHIFT correction effectively aligns peaks of pulses to near that of the template, it is independent of changes to the trigger threshold. However, the position of the peak of the template relative to the time origin of it is dependent on the trigger threshold used at the time the template was computed. Thus, the adjusted trigger time with the TICK_SHIFT correction relative to the true onset of the pulse remains dependent on the thresholds used at the time of template generation. This means that, if changes of the thresholds between the template generation and observations are different between pixels, that can make pixel-dependent offsets on the trigger times after the TICK_SHIFT correction. Thus, the timing coefficients should have separate values for each pixel.

Another anticipated characteristic is energy dependence. A large, initial energy dependence of trigger times due to applying a uniform trigger threshold is corrected by TICK_SHIFT. However, there is another source of the energy dependence of timing, which is the non-linearity of the pulse shape. For higher energy x-rays, the time interval between the rise and maximum of the derivative is slightly shorter. Therefore, the trigger times (corrected for TICK_SHIFT) are slightly later for higher energy x-rays. Thus, the timing coefficients should have a term to correct the energy dependence.

Based on the three types of dependence (grade, pixel, and energy), the time coefficients are formalized as follows:

$$\mathrm{SAMPLECNT} = \mathrm{SAMPLECNTTRIG} - (A * \mathrm{RISE\_TIME}/4.0 + B * \mathrm{DERIV\_MAX} + C)$$

Here, SAMPLECNTTRIG is the Resolve local time corresponding to the trigger time. SAMPLECNT is the analogous quantity for calibrated photon arrival times. Both are in units of 80 μs, and have 5 μs resolution. A, B, and C are the timing coefficients. Both the terms involving A and B implicitly describe the energy dependence because both rise times (RISE_TIME) and maximum derivatives (DERIV_MAX) of pulses are approximately proportional to pulse amplitudes and therefore to x-ray energies. Practically, we only need either one (A or B) to correct the energy dependence. In fact, for SXS, this dependence is fully included in the B coefficient and the A coefficient was set to 0 (Section 2), but both coefficients are kept for flexibility/redundancy. C is a constant term. Grade and pixel dependence are corrected by having different values of the coefficients, primarily in C, for different grades and pixels. For Resolve, there are separate columns for the five grades, for instance, AHP, AMP, AMS,

ALP, and ALS for the A coefficient, so there are 15 columns in total for A, B, and C. Each of these is a 36 element array, one per pixel. These are all stored in a single row of the ARRCOEFFS extension. If we need to apply different timing coefficients for different observation epochs, e.g., in response to an update of the template, a new row containing a new set of the coefficients can be added. The TIME column in this extension stores the start of the applicable observation time frame for each row. Because the time coefficients depend on the optimal filter templates in use, the extension also has the SHPTEMPL column, which provides a short string ID representing the set of the templates used during the applicable observation time frame. Note that the related ftools use the TIME columns only to query the time coefficients and the SHPTEMPL is only for reference. The string ID stored in SHPTEMPL is the creation date of the templates. This ID is also in the header of the calorimeter pixel event FITS files. Further descriptions for the SHPTEMPL values are given in the RSLTHRES extension of the CONFTHRE CALDB ([4]).

DELTIMES

The first three parameters in the DELTIMES extension (DTPRIMARY, DTMIDHIGH, and DTLOWMID) are time intervals to determine grades of triggered events (ITYPE=0-4). Event grades are assigned onboard by the PSP, but can be recalculated using these parameters and the rslsecid ftool, if needed. The values are set to those used in the PSP, and do not need further study (however, only the initial delivery has different values, see Section 2.4). Here, we briefly describe how the values were chosen.

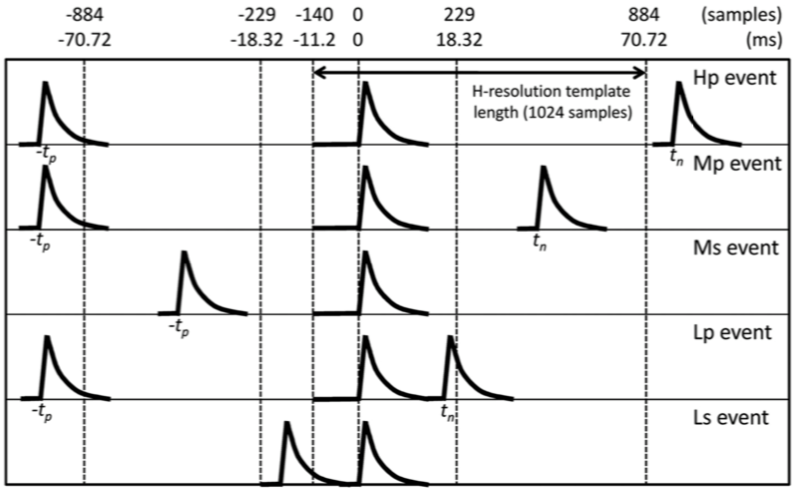

Figure 2 Schematic view of grade definitions for pulses arriving at time t=0 (taken from [2]). The time interval t_p denotes that to the previous pulse, while t_n denotes that to the next pulse.

Figure 2 illustrates how the event grades are defined. The event grades consist of two concepts: how much an event is close to the nearest one (H-, M-, or L-res); and whether an event is preceded by others (secondary: s) or not (primary: p) within a certain time interval. To perform the optimal filtering, an event should be distant enough from others, so that the pulse sample (excluding the pre-trigger part) does not overlap with pulses of adjacent events. For H-res events, the full-size (1024 samples) template is convolved with the whole pulse record including 140 pre-trigger samples, thus the minimum separation required to be H-res (defined as `DTMIDHIGH` in CALDB) is (1024–140) samples = 70.72 ms. For M-res events, a shorter template covering 256 samples with 27 pre-trigger samples are used, and the minimum separation (`DTLOWMID`) is (256–27) samples = 18.32 ms. `DTPRIMARY` is the time interval used to distinguish primary and secondary events. This time interval is set to be the same as `DTMIDHIGH`. Therefore,
`DTPRIMARY = DTMIDHIGH` = 70.72 ms,
`DTLOWMID =` 18.32 ms.

Other time intervals in this extension define time windows to mark coincidence between events. Different time window parameters are defined for various types of coincidence, each optimized for a different source (or sources) of non X-ray events (see [5] for details). The coincidences flagged by `rslflagpix` uses the `TIME` column of event files, which means that coincidences are evaluated using photon arrival times calibrated with A, B, and C as described above. Therefore, these time intervals may need to be checked, but not necessarily revised for each update of the A, B, and C coefficients. Coincidence flags are written back to the `STATUS` column of calorimeter pixel event files, which has multiple values (bits), one (or more in some cases) for each coincidence type.

`CTRECDT` stores the time interval that identifies background events originating from cal-pixel recoil electrons. Events occurring within ±`CTRECDT` of a cal-pixel event are flagged by `rslflagpix` if the event pair also satisfies a check as to whether the energies are consistent with being a recoil pair of a Mn Kα or Mn Kβ photon. Two `STATUS` bits are used by `rslflagpix`: one is raised if the time coincidence is satisfied; and the other is raised if both the time coincidence and the energy check are satisfied.

`PROXDT` is similar, but applies to any two pixels and has no energy check, in that it flags tightly correlated pairs of events, such as from an electron lost from one pixel and absorbed by another, or non-x-ray events due to thermal disturbance by cosmic rays hitting the thick Si layer around the detector array (frame events). The reason to have separate intervals for coincidence with cal-pixel events (`CTRECDT`) and other-pixel events (`PROXDT`) is that pairs involving the cal pixel are primarily due to calibration source x-rays, thus the pulses are similar with normal `RISE_TIME` values, and the coincidence window may be kept small. On the other hand, for `PROXDT`, frame events have slow `RISE_TIME` and thus a large spread in effective photon arrival times, which may require a larger coincidence window.

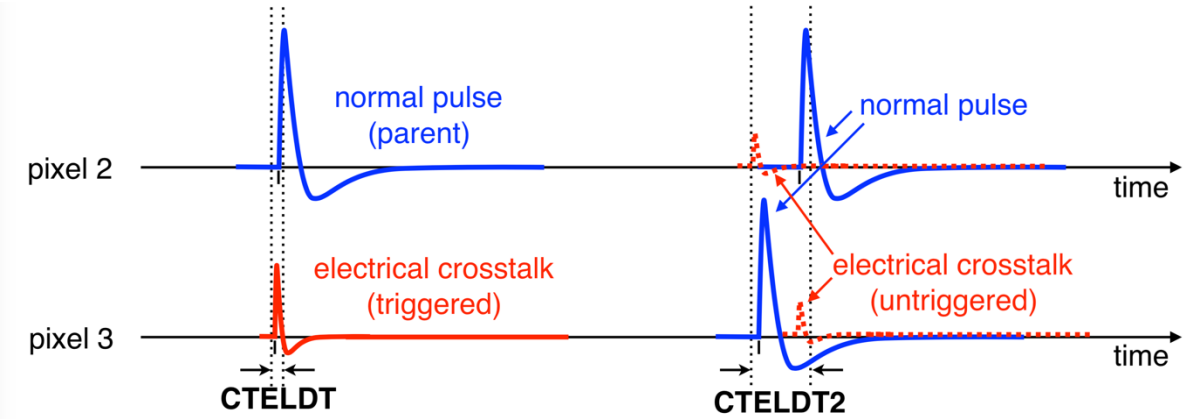

Figure 3 A schematic of triggered (left) and untriggered (right) electrical crosstalk. See the text for the details.

`CTELDT` stores the time interval between events required for triggered electrical crosstalk events to be flagged by `rslflagpix`. `CTELDT2` stores the time interval between events that could be contaminated by untriggered electrical crosstalk. An x-ray event in a given pixel can cause cross-talk in electrical neighbors, with the largest effect on the electrical nearest neighbors, and a much smaller effect on more distant neighbors. `CTELDT` and `CTELDT2` are applied to pairs of pixels that are electrical neighbors, and users can choose how many neighbors to include in calculating the coincidences using the parameters `ctelnear` and `ctelnear2` in `rslflagpix`. Note that only 1 and 2 are possible values for these parameters. The default setting is to consider only nearest neighbors (`ctelnear` = `ctelnear2` = 1). `Rslflagpix` sets two bits of the `STATUS` column of pixel event files for each of `CTELDT` and `CTELDT2`: one is raised if an event is involved in a time-coincident, electrical neighbor pair; and the other is raised if an event has the largest `PHA` in the pair. Electrical crosstalk has a smaller and faster pulse than a normal event. Thus, for triggered crosstalk, events with the first bit raised but not the second bit should provisionally be considered as crosstalk events. On the other hand, events with both bits raised are likely parental, normal events, which do not need to be discarded. For example (Figure 3, left), if a small event on pixel 3 occurs within `CTELDT` of a normal pulse event on pixel 2 (one of the nearest electrical neighbors of pixel 3), then both bits are raised for pixel 2, meaning the event at pixel 2 is likely a normal event, while only the first bit is raised for pixel 3, indicating this event is due to electrical crosstalk from pixel 2. In practice, the pulse height (`PH`) and rise time (`RISE_TIME`) should be sufficient to identify it as such (see Section 2.3). For untriggered crosstalk, another set of two bits of the `STATUS` column is used in the same way as triggered crosstalk. However, in this case both events in a pair should be regarded as crosstalk candidates because the energy assignment of both events may be contaminated (Figure 3, right), and thus the bit distinguishing `PHA` rank should not be used. Note that the screening using `CTELDT2` flagging should never be used for L-res events, because the `PH` for L-res is only obtained from the peak. In principle, one might define a smaller coincidence window for L-res only; however, this is currently not implemented.

For each of all these pixel-to-pixel coincidences, a lower threshold is set on pulse heights of events using the pxpithr parameter; i.e., if the calibrated pulse height (PI) of an event is smaller than the value of this parameter, that event is skipped in the processing of coincidences in rslflagpix. The pxpithr parameter is a vector of four values, one per each coincidence type. Pulse heights of triggered electrical crosstalk events are smaller than their parental events by a factor of ~50. The pxpithr values for recoil and proximity crosstalk should be sufficiently high so that the software ignores most of triggered electrical crosstalk events that could otherwise contaminate other types of pixel-to-pixel coincidences. On the other hand, the pxpithr value for triggered electrical crosstalk events should be low enough not to skip them.

The last set of the time intervals are for coincidence flagging with anti-co. The values ANTDTPRE and ANTDTFOL define the lower and upper limits of the coincidence screening window, where ANTDTPRE (ANTDTFOL) is the time interval preceding (following) each anti-co event. Because rslsamcnt and xatime do not transform raw anti-co trigger times to calibrated arrival times, whereas the corresponding calorimeter pixel event times are calibrated, the value ANTSHIFT is applied to shift each anti-co trigger time prior to using ANTDTPRE and ANTDTFOL to calculate the coincidence window. In rslflagpix, to reduce the false coincidence rate, thresholds are set for minimum pulse heights and durations (PHA and DURATION, respectively) of anti-co events used in the flagging, which can be specified with the antphathr and antdurthr parameters. For example, if an anti-co event has a smaller pulse height than antphathr, it is skipped in rslflagpix, and no calorimeter pixel events are flagged for this anti-co event, even if there are pixel events within the coincidence window.

As in ARRCOEFFS, the additional TIME column in the CALDB defines applicable observation time intervals. Each row corresponds to an applicable observation time frame, and has a single value for each of the pixel-to-pixel coincidence parameters (CTRECDT, PROXDT, CTELDT, and CTELDT2). Because optimized values of the anti-co related time window parameters depend on the triggering threshold for the anti-co events, the threshold values are stored in the DEVPTHAC column in DELTIMES. As for SHPTEMPL in ARRCOEFFS, DEVPTHAC in DELTIMES is only for reference and not used by the related ftools to query the time window parameters. The detailed description of the DEVPTHAC values, together with the threshold values for the calorimeter pixels (DEVPTHPX) used in combination, are given in the RSLTHRES extension of the CONTHRE CALDB ([4]). Although there is only one physical anti-coincidence detector, it has two separate readouts at the PSP A and B sides. Therefore, in the columns for the coincidence with anti-co (ANTSHIFT, ANTDTPRE, and ANTDTFOL), each row has two separate values for the two PSP sides. Users can choose which side should be used in rslflagpix (the A side is default). Similarly, each row of the DEVPTHAC column has two values for the two PSP sides, as the anti-co triggering threshold can have different values for the sides A and B.

Note that, in `rslflagpix`, any of these time window parameters can be overridden by explicitly specifying the values in units of seconds as arguments with identical parameter names to the column names.

2 Revision 20190621 (First delivery)

CalDB Filename	Validity date	File(s) as delivered	Delivery date	Comment
none	20190101 00:00 UT	rsl_coeftime_20190621.fits	20190621	Values from Hitomi/SXS.

2.1 Data Description

The data in this release is identical to that used in the final release of the SXS timing coefficients CALDB (but see also section 2.4 for the changes made in the file format). The description of the analysis and results in this document are based on those reported in [6].

Data Description: ARRCOEFFS

Systematic timing differences associated with the pixel channel number (`PIXEL`) were determined by analysis of detector pulse records of filter wheel ^{55}Fe events collected during the thermal vacuum testing on June 25, 2015. These differences were not revised with in-orbit data.

The energy dependence, i.e., dependences on event pulse rise time (`RISE_TIME`) and/or derivative peak (`DERIV_MAX`), was initially evaluated using cosmic ray events collected on June 21 and 25, 2015, and later revised with the in-orbit data of the Crab pulsar, observed on March 25, 2016. In the Crab analysis, we used the radio ephemeris derived from the simultaneous observations using Tohoku University 30 m (325 MHz) and Kashima 34 m (1.4-1.7 GHz) telescopes conducted by T. Terawasa's group at ICRR/University of Tokyo.

Event-grade (`TYPE` or `ITYPE`) dependence was initially determined by analysis of data obtained during Spacecraft integration testing in 2015. The data were collected using the Modulated X-ray Source (MXS) during the ASTRO-H integration testing: the SXS comprehensive test on May 19, 2015, the system function test (FNC-D) on May 21-22, 2015, and the thermal vacuum test (Tvac) on June 26-27, 2015. Since the gate valve (GV) was closed during each test, and its support structure partially obscured the MXS beam, 27 of 35 pixels were not illuminated by the MXS. The values were revised after the launch using folded light curves of the Crab pulsar observed on March 25, 2016. All pixels were able to receive X-rays from the telescope even when the GV was closed, as it was on that date.

Data Description: DELTIMES

Cosmic ray events collected on June 21, 2015, acquired with no x-ray illumination and with pulse derivative thresholds of 120, were used to characterize the time intervals between correlated pairs of calorimeter events (not involving electrical crosstalk). The results were re-evaluated in orbit during the observation of RX J1856.5–3754 on March 17, 2016. This source has a soft spectrum and was effectively a background exposure for the SXS, since the low energy photons of RX J1856.5–3754 were absorbed by the GV Be window.

Similar cosmic ray events collected on May 19, 2015 prior to FNC-D test with low pulse derivative threshold of 25, were used for initial study of the timing of electrical crosstalk. The result was re-evaluated with the in-orbit background data from the observation of RX J1856.5–3754 on March 17, 2016, and the observation of the Crab pulsar on March 25, 2016. The dependence of pulse-height determination of a pulse contaminated by undetected electrical crosstalk on the separation in time of that crosstalk was determined by modeling and verified via analysis of MXS data (e.g., in the nominal operation test and FNC-D on November 10-11, 2015).

Cosmic ray events observed with SXS on May 18, June 21, and June 25, 2015 and the in-orbit background data from the observation of RX J1856.5–3754 on March 17, 2016 were used to characterize the anti-co timing relative to the calorimeter pixels.

2.2 Data Analysis

All ground testing data were analyzed with Igor Pro version 6.37 with the XRSGSE software and all in-orbit data were analyzed using ftools XRONOS package version 5.22. The barycentric correction was applied to the Crab data using the `barycen` ftool with the orbit file and the target coordinates of $(\text{R.A., Decl.})_{J2000.0}$ = (83.6332 deg., 22.0145 deg.) before the folding analysis described below.

Data Analysis: ARRCOEFFS

As described in Section 1.3, the pixel-to-pixel differences in trigger times originate from the `TICK_SHIFT` correction. Thus, this difference is only found in the trigger times of H- and M-res grades. On the other hand, the `DERIV_MAX` time (used as the trigger times for L-res events) is not affected by `TICK_SHIFT`, and it is expected to be pixel independent. Thus, systematic comparison of the telemetered trigger time with the `DERIV_MAX` time for each event allows us to evaluate the pixel-to-pixel differencs in trigger times for H- and M-res grades. Although the `DERIV_MAX` time is not calculated onboard for H- or M-res events, it can be calculated using pulse record dumps. About 100 pulse record dumps of the ^{55}Fe data of predominantly H-res

events were analyzed for each pixel. The DERIV_MAX times were calculated with the PSP algorithm using a boxcar derivative.

For the energy dependence (RISE_TIME and DERIV_MAX dependence), we decided to use the B coefficient only and set A = 0 for all grades and pixels because RISE_TIME and DERIV_MAX are well correlated to each other for those have good RISE_TIME values (~40-60, in units of 20 μs) in the standard screening, and therefore the correction of one dependence inevitably compensates the other dependence implicitly. We chose to correct the DERIV_MAX dependence rather than RISE_TIME, because RISE_TIME is noisier for low energy pulses than DERIV_MAX.

The analysis of the Crab pulsar data for the energy dependence, grade dependence, and absolute timing was done by measuring the lag of the first peak in the folded light curve. The folding parameters were determined with the radio ephemeris from the simultaneous observations [7][2]:
Epoch (MJD–40000) = 17472.000000287430393518 51 (0.2 μs),
Period = 3.3720439605e–02 s (4e–12 s),
Derivative of period = 4.19808934213565347e–13 s s^{-1} (~1e–18 s s^{-1}),
where the values in the parentheses show the uncertainties.

We first determined the B coefficient. In principle, the first peak lag can be measured for each pixel, but the energy dependence is expected to be the same between the pixels. Besides, the statistics of the Crab pulsar data were not sufficient to perform pixel-by-pixel measurements of the lag. Therefore, we corrected the pixel-to-pixel difference of trigger times beforehand based on the ground results, and merged the data for all pixels. The data were then divided into the three major grades (H-, M-, and L-res or ITYPE = 0, 1-2, and 3-4) and three different DERIV_MAX ranges: 100-2600, 2600-5100, and 5100-7600, roughly corresponding to 0-4, 4-8, and 8-12 keV, respectively. For each of the major grades, the B coefficient was determined by measuring the lag as a function of DERIV_MAX. After that, using the data corrected for the DERIV_MAX dependence, the first peak lags were re-evaluated to measure offsets between grades and that from an absolute time reference, both compensated by the C coefficient. It is known that the first x-ray pulse peak leads the corresponding radio peak by 314.6±5.4 μs [8]. The C coefficient values were determined so that the first peak aligns at the reference point set by the radio peak in the simultaneous observation corrected for the radio delay.

In the ground measurements of the energy (DERIV_MAX) dependence, we used the relative timing of calorimeter pixel events to those of the associated with anti-co events (within a 1.5 ms time window). The anti-co trigger times slightly depend on anti-co event energies (with dispersion of ~100 μs), but hardly depend on the energies of associated calorimeter events. The

[2] This radio ephemeris shown here is slightly different from that listed in [7]. This is because there were two versions: quick-look, tentative result which we used for the SXS absolute timing calibration, and final result used in [7]. The difference is small enough compared to the absolute timing requirement for SXS (1 ms).

latter characteristic makes the anti-co trigger time a good reference to evaluate the energy dependence of the trigger times of the associated calorimeter pixel events. Since the statistics were high, the distribution of pixel-to-anti-co times was directly fit by a linear function of DERIV_MAX to derive B. The ground measurements of the grade dependence used the same technique as for the pixel-to-pixel difference; the DERIV_MAX times were calculated for H/M-res events, and the systematic difference from the trigger times was measured, assuming that the DERIV_MAX times represent the trigger times for L-res events.

For Resolve, we plan to use pulse record dumps to evaluate all the dependences on pixels, grades, and energies of trigger times. As demonstrated by [9], the dependence on energy can directly be measured using amplitude-normalized, TICK_SHIFT-corrected pulse derivative curves (i.e., those shown in the bottom panel of Figure 1). Therefore, we expect that all the A, B, and C coefficients can be determined using pulse record dumps of cosmic ray events, except for the absolute term of C. In-orbit calibration using an astrophysical source like the Crab pulsar is still necessary to determine the absolute timing. Another limitation of the calibration method using pulse record dumps is that statistics for secondary events would probably be insufficient. Therefore, in-orbit data of an astrophysical source would also be important to check possible differences in the coefficients between primary events and secondary events (Mp vs. Ms and Lp vs. Ls).

Data Analysis: DELTIMES

The time interval statistics to determine the coincidence windows were obtained by clustering event groups that were correlated in time, with different data filtering optimized for each coincidence type, as described below.

For pixel-to-pixel pairs not involving electrical crosstalk, i.e., electron recoil pairs and frame events, low-energy events (below 100 eV and 150 eV for the ground and in-orbit data, respectively) were removed to avoid confusing the study with electrical crosstalk. The ground data set was suitable for evaluating CTRECDT because the rate of cosmic ray events (mainly due to sea-level muons) was much lower than in orbit, and the contribution from frame events was negligible. Thus, cal-pixel events were kept for the ground data. On the other hand, the in-orbit data set was mainly used to evaluate PROXDT, and cal-pixel events were removed to reduce the rate of false coincidence. For each of the data sets, correlated events within a 1.5 ms time window were clustered and time intervals of clusters were evaluated.

For electrical crosstalk between pixel channels, the data from all pixels including the cal pixel were analyzed to evaluate CTELDT and CTELDT2. Crosstalk groups were identified by clustering electrical neighbor events correlating within a 1.5 ms time window.

For cosmic ray events, calorimeter pixel events associated with anti-co events (within 1.5 ms time window) were analyzed. The centroid, left- and right-side extents of the distribution of the pixel-to-anti-co relative times were used to determine ANTSHIFT, ANTDTPRE, and ANTDTFOL, respectively.

2.3 Results

Results: ARRCOEFFS

The observed offsets between H/M-res vs. L-res and H-res vs. associated anti-co event times peaked at 930 μs and –200 μs, respectively. However, the offsets of pixel 26 were 130 μs later for the both offsets (800 μs and –360 μs, respectively). This is explained by the fact that a higher threshold (62) was used for pixel 26 compared to others (24-26 for most pixels) when templates were generated due to high-frequency ringing on pixel 26. Thus, the time reference for pixel 26 is later than for the other channels (and thus closer to the L-res timing determined at DERIV_MAX). This timing offset for pixel 26 is compensated by the C coefficient. Offsets between the other pixels were usually much smaller than 1 sample count (80 μs), and a common C value was used for each grade between these pixels.

We set the A coefficient to be 0 for all grades:
AHP = AMP = AMS = ALP = ALS = 0

The B coefficient was derived to be:
BHP = –(1.563 ± 1.171)e–04,
BMP = BMS = –(1.048 ± 0.886)e–04,
BLP = BLS = –(3.329 ± 0.924)e–04,
in units of (80 μs sample) / (1 DERIV_MAX step). The best-fit value of each parameter is smaller (larger in the absolute value) than the ground test results, but still consistent within the statistical error of the Crab results. In SXS, it was not expected that coefficients were different between primary and secondary events, thus BMP = BMS and BLP = BLS were assumed (see also Section 2.4).

For the grade dependence compensated by the C coefficient, we found a 930 μs difference between H/M-res and L-res timing in the ground measurement as described above. We also observed a consistent offset between the grades (450 μs for H/M-res vs. 1360 μs for L-res) in the delay of the actual MXS x-ray arrival time from the time of MXS illumination on command. In the in-orbit measurement using the Crab pulsar, the offsets of M-res and L-res from H-res were ~10 and ~900 μs, respectively, consistent with the ground results. The C coefficient also compensates the offset from the absolute reference. For H-res, the offset of H-res from the absolute reference was ~417 μs.

The resultant C values, considering the grade and pixel dependence as well as the absolute timing were obtained to be:
CHP = 5.215±0.203 (for all but pixel 26), 6.840±0.203 (for pixel 26),
CMP = CMS = 5.345±0.141 (for all but pixel 26), 6.970±0.141 (for pixel 26),
CLP = CLS = 17.296±0.142 (for all pixels),
in units of 80 μs. The uncertainties are the statistical errors in the fitting deriving the first lag peak. Again, the same coefficients were assumed between primary and secondary events. For Resolve, we plan to measure values separately for primary and secondary events using the Crab pulsar or a similar astrophysical calibration source.

The correction result with the A, B, and C coefficients evaluated with the Crab pulsar's first peak is shown in Figure 4.

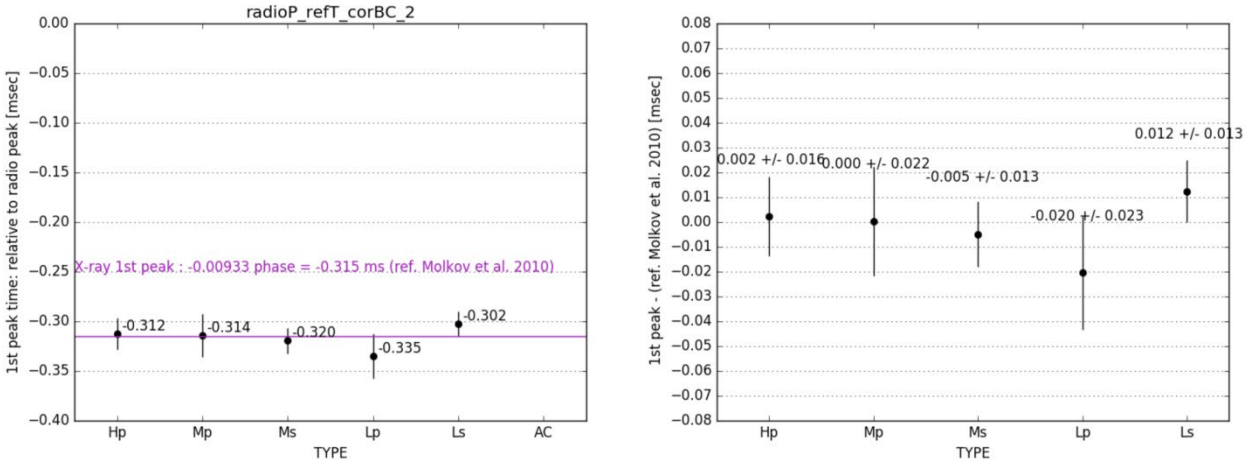

Figure 4 Left: Comparison of the first peak lags after the correction using the A, B, and C coefficients (dots) with the reference time (magenta; [8]). Right: Residuals from the reference. Error bars in this plot are dominated by the statistical errors of the SXS data but also includes a minor contribution from that of the RXTE/PCA data (~6 μs; [8]) added in quadrature.

Results: DELTIMES

For pixel-to-pixel pairs not involving electrical crosstalk, the ground and in-orbit data showed different distributions of the time intervals Figure 5; the red histogram in left and the green histogram in right, respectively). This is primarily due to additional contribution from frame events in orbit.
First, we determined CTRECDT using the histogram of the ground data. The most probable time interval of correlated pairs was 0, with a standard deviation of 38 μs. CTRECDT was set to 0.24 ms, to cover most of the observed distribution and to be a integer multiple of one time sample (80 μs). Note that we did not separate pairs involving the cal-pixel from those that did not, given the limited statistics of the ground data.

Next, we evaluated PROXDT using the in-orbit data. The right panel of Figure 5 shows histograms of time intervals between consecutive events with different event selection on RISE_TIME: (0) all event pairs with any RISE_TIME values, (1) only event pairs with at least one good RISE_TIME, and (2) only event pairs both with good RISE_TIME. In this study, the good range of RISE_TIME was set to 42-56. Pairs both with good RISE_TIME (the blue histogram in Figure 5, right) are mostly electron-lost-and-found events. In fact, the required time interval to cover this histogram is consistent with CTRECDT determined on ground (CTRECDT is defined for the cal-pixel recoil event pairs, but the time intervals are expected to be similar to each other between cal-pixel recoil pairs and non-cal-pixel recoil pairs because the physical process is the same). Pairs involving bad RISE_TIME, presumably frame events, require significantly larger time intervals (green and red vs. blue in Figure 5, right). Those with both events having bad RISE_TIME (included in green only) do not need time-coincidence screening as these are removed by the screening on RISE_TIME. Thus, PROXDT only needs to cover event pairs in the red histogram, and was set to 0.72 ms. Again, the value was chosen to be a integer multiple of a time sample (80 μs).

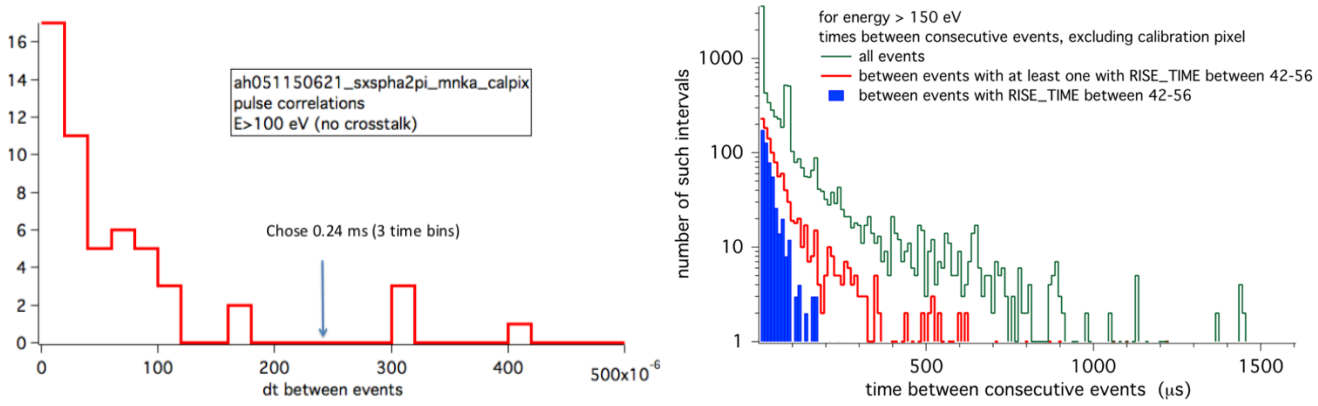

Figure 5 Interval statistics for non-electrical crosstalk, pixel-to-pixel pairs. Left: ground measurement including pairs involving the cal-pixel. Right: In-orbit measurement using the "blank sky" data of the RX J1856.5–3754 observation, cal-pixel events excluded. Colors in the right panel show the results of different event cuts: (0) all event pairs with any RISE_TIMEs in green, (1) only event pairs with at least one good RISE_TIME in red, and (2) only event pairs both with good RISE_TIMEs. The right panel is taken from [5].

For electrical crosstalk, only event clusters of the electrical nearest neighbors were studied, because more distant neighbors are much less affected by crosstalk (Section 1.3). Since each pixel has one or two electrical nearest neighbors, identified clusters were electrical doubles or triples, each consisting of a primary source event and one crosstalk candidate, or a primary source and two crosstalk candidates, respectively. The observed time intervals within crosstalk doubles and triples from the in-orbit data are shown as a histogram in Figure 6. Because the shape of crosstalk is very different from normal (thermal) pulses, the time assignment is not robust. Relative to primary events, crosstalk would need to be flagged within the window of –1 ms (Figure 6), and CTELDT was set to 1.0 ms. However, timing is not needed to identify electrical crosstalk. Crosstalk appears at smaller RISE_TIME than normal pulses, and smaller

pulse heights (PH). The gain scales of all grades map electrical crosstalk pulses from typical x-ray events to energies below 100 eV. Thus, energy discrimination easily removes most crosstalk, and rise time discrimination will remove rare crosstalk events from unusually large PH events. In SXS, triggered electrical crosstalk was removed by these screenings, and CTELDT was only a placeholder. The cut using the time coincidence flagging with CTELDT was not applied for electrical crosstalk in the standard screening.

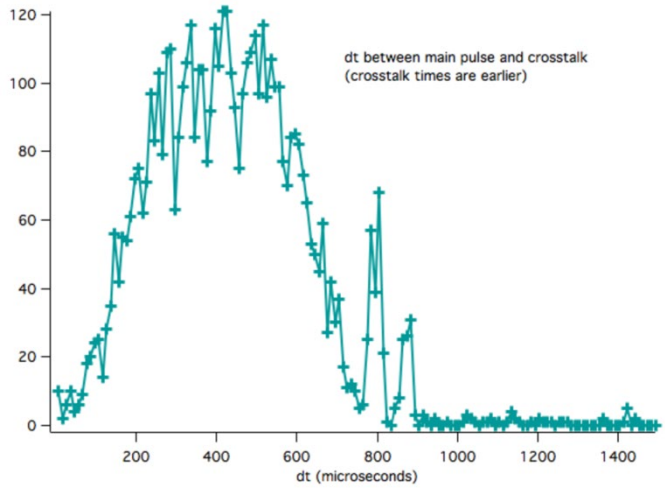

Figure 6 Statistics of time offset between the primary pulse and triggered electrical crosstalk.

Untriggered crosstalk needs additional consideration. The presence of a crosstalk pulse on an x-ray pulse will alter the energy that the PSP determines for that pulse. Computing the impact of the crosstalk from an 8 keV x-ray on a normal x-ray pulse as a function of displacement from the arrival time of the x-ray event, we determined that the error could be kept to < 0.5 eV if the coincidence window of ±25 ms for electrical nearest neighbors was excluded, with the exception of a very small window of enhancement if a crosstalk pulse arrives in the last 2 ms of a pulse record, due to non-zero power in the filter at the end of the template. The results of this modeling agree with the MXS data taken during the ground measurements, for which the pulsed output increases the probability of pulses occurring on adjacent pixels within the pulse time. Thus, we set CTELDT2 = 25 ms. In SXS, the cut using the time coincidence flagging with CTELDT2 was not applied in the standard screening because we did not see any significant impact due to untriggered crosstalk. The observations had rates that were much lower than that of pulse-on durations of the MXS data, and thus too low to matter.

2.4 Remarks

This is the first delivery for the coeftime CALDB file. The data is based on the Hitomi/SXS results. No CALDB file was released pending minor updates; see Section 3. Although the values

have not changed from Hitomi, the CALDB format has been updated. Following is the list of the updates.

- In SXS, the A, B, and C coefficients had a single column for each of the major three grades (`AH`, `AM`, and `AL` for H, M, and L-res, respectively, in the case of A, for example), and the differences between primary and secondary events were attributed to different extensions (`ARRCOEFFS` and `ARRCOEFFSSEC`, respectively; however, these two contained the same values, and the software, `sxssamcnt`, never used `ARRCOEFFSSEC`). For Resolve, these are merged into one extension, `ARRCOEFFS`, and separate columns are defined for primary and secondary events, as described in Section 1.3.
- The anti-co parameters, `ANTDTPRE`, `ANTDTFOL`, and `ANTSHIFT`, are now defined separately for the two PSP sides, which were either single values (`ANTDTFOL` and `ANTDTPRE`) or could have two values but the software had no capability to choose a correct side for each pixel-to-anti-co coincident event pairs (`ANTSHIFT`).
- In SXS, an additional parameter `MXSDT` was included. This stored a time interval of the afterglow of the MXS, which was used to calculate good-time intervals for MXS on and off periods. Since it has been learned after the Hitomi misson that the afterglow interval depends on the MXS operating parameters, this single parameter has been upgraded to a series of tables and separated to a new CALDB file identified by the string “mxsparams.” For details on this CALDB file, see [10].

Another remark is warranted on the time intervals for event grading, DTPRIMARY, DTMIDHIGH, and DTLOWMID. In the early development and testing of the PSP, it used longer pre-trigger lengths of 150 samples = 12.00 ms (instead of 140 samples = 11.20 ms) for H-res, and 37 samples = 2.96 ms (instead of 27 samples = 2.16 ms) for M-res, which resulted in smaller time intervals, DTPRIMARY = DTMIDHIGH = 69.92 ms and DTLOWMID = 17.52 ms (see e.g., [11]), than what was actually used by the PSP in orbit (70.72 ms and 18.32 ms, respectively; see [2] and Section 1.3). The update of the values was not reflected in the timing CALDB for SXS as seen in [6] because of mis-communication between the instrument team and software calibration team at that time. Since the initial delivery of the timing coefficients for Resolve is a copy of the Hitomi/SXS results, this release also includes the obsolete values for these time intervals, which we plan to update in the next delivery, to reflect the pre-trigger lengths used in orbit for Hitomi/SXS and planned for Resolve. In this first delivery, the CALDB file does not have either the `SHPTEMPL` column in the `ARRCOEFFS` extension or the `DEVPTHAC` column in the `DELTIMES` extension because it was decided after the first delivery to append these to this CALDB (see Section 3).

3 Revision 20200120

CalDB Filename	Validity date	File(s) as delivered	Delivery date	Comment
xa_rsl_coeftime_20190101v001.fits	20190101 00:00 UT	rsl_coeftime_20200120.fits	20200120	Minor bug fix of values and update of the format

3.1 Data Description, analysis, results, and remarks

No new measurement or data. This delivery corrects minor bugs in the grade defining time intervals, DTMIDHIGH, DTLOWMID, and DTPRIMARY in the DELTIMES extension. As described in Section 2.4, the first delivery (and the CALDB for Hitomi/SXS) used slightly wrong values for these three time intervals. In this delivery, the values are corrected to those actually used in-flight by the Hitomi/SXS PSP and planned for Resolve. The comparison of old and new values is shown below.

Old (the first delivery on 20190621, the same as the Hitomi/SXS CALDB):
DTPRIMARY = DTMIDHIGH = 69.92 ms,
DTLOWMID = 17.95 ms.

New (this delivery on 20200120, the same as the values in Section 1.3):
DTPRIMARY = DTMIDHIGH = 70.72 ms,
DTLOWMID = 18.32 ms.

This delivery also adds two reference columns (SHPTEMPL in ARRCOEFFS and DEVPTHAC in DELTIMES; see Section 1.3 for the details). The values of the new columns are taken from the current version of the CONFTHRE CALDB. See [4] for the details.

4 Revision 20230331

CalDB Filename	Validity date	File(s) as delivered	Delivery date	Comment
xa_rsl_coeftime_20190101v002.fits	20211213 06:54 UT	rsl_coeftime_20230331.fits	20230331	Updates were made for [ARRCOEFFS] All parameters [DELTIMESANT_*

4.1 Data Description

Data Description: ARRCOEFFS
Data Description: DELTIMES

For this version of the CALDB, we used the following data sets obtained in the ground test in JAXA's Tsukuba Space Center after 2021 December when the flight optimal filter templates were implemented (Table 3).

Table 3 Resolve ground data set used for this version of the CALDB updates.

	Verification level	Major tests	Start	Stop	50 mK time (Ms)
TC5	Instrument-level	Calibration, etc.	2022-01-27	2022-03-12	2.2
TC6	Spacecraft-level	init. elec. test	2022-06-05	2022-06-17	0.9
TC7	Spacecraft-level	thermal-vacuum	2022-07-17	2022-08-29	2.4
TC9	Spacecraft-level	final elec test	2023-02-06	2023-02-14	0.3

We processed the data using the pre-pipeline and pipeline processing, which are based on the flight equivalent with some modifications to fit with the *Resolve* ground testing data. We removed events out of the stable 50 mK temperature control. The resultant exposure times were 5.8 Ms. We applied the minimum screening with the following.

- QUICK_DOUBLE=0
- SLOPE_DIFFER=0
- -8 < TICK_SHIFT <7

As described in Section 1, the relative timing can be determined using several methods using the MXS, anti-co, and pulse record data. We used combinations of them. For each method, we used appropriate subsets of the data, which is described in Section 4.2.

4.2 Data Analysis & Results

Data Analysis: ARRCOEFFS

The relative timing is characterized by the "A", "B", "C" parameters, which are applied as

SAMPLECNT[g, p] = SAMPLECNTTRIG [g, p] – (A [g, p] * RISE_TIME/4.0 + B [g, p] * DERIV_MAX + C [g, p]),

in which A [g, p], B[g, p], and C[g, p] depend on the grades (Hp, Mp, Ms, Lp, and Ls) and the pixels (0-35). The total number of the parameters is 3*5*36=540. This is too flexible, and we use the following constraints in the same way as SXS.

1. A [g, p] = 0, as the RISE_TIME and DERIV_MAX are strongly correlated, hence B [g, p] alone can represent the timing delay.
2. B [g, p] = B [g, 0]; i.e., there is no pixel dependence on B.
3. B [Mp] = B [Ms] ; i.e., B is common between Mp and Ms.
4. B [Lp] = B [Ls] ; i.e., B is common between Lp and Ls.
5. C [Mp, p] = C [Ms, p]; i.e., C's are common between Mp and Ms.
6. C [Lp, p] = C [Ls, p] ; i.e., C's are common between Lp and Ls.

Instead, for the analysis purposes, we introduce the "D" parameter as in

SAMPLECNT[g, p] = SAMPLECNTTRIG [g, p] – (A [g, p] * RISE_TIME/4.0 + B [g, p] * DERIV_MAX + C' [g, p] + D),

in which C [g, p] = C' [g, p] + D. In other words, C [g, p] is decomposed into the term for the absolute timing and the term relative to it. We define C'[Hp, 0] = 0. Note that this decomposition is only for the analysis purpose here; C[g, p] = C' [g, p] + D is included in the CALDB.

With these rearrangements, the total number of the parameters is 3 (B[H/M/L]) + 3*36 (C'[H/M/L, p]) -1 (C'[Hp, 0]) + 1 (D) = 111. They are derived in the following analysis (1)-(5).

Analysis (1) B[H] and C'[H, p]

The details of this analysis are described in Omama et al. (2022). Here, we provide excerpts. We used the MXS data taken during TC6 using MXS. The nominal and redundant sides of the direct MXS (MXS1 and MXS3, respectively) illuminate the complementary half of the array when the gate valve is closed (Figure 7). We used the data set of the two side illumination.
An example of the spectrum and the folded light curve is shown in Figure 8.

(a) MXS1 (b) MXS3 (c) MXS1+3

Figure 7 Count rate (1/s) distribution of the MXS1 (nominal side), MXS3 (redundant side), and both sides together using a data set in TC6. Note that the count rate for pixel 12 is by the ^{55}Fe calibration source, not by the MXS [13].

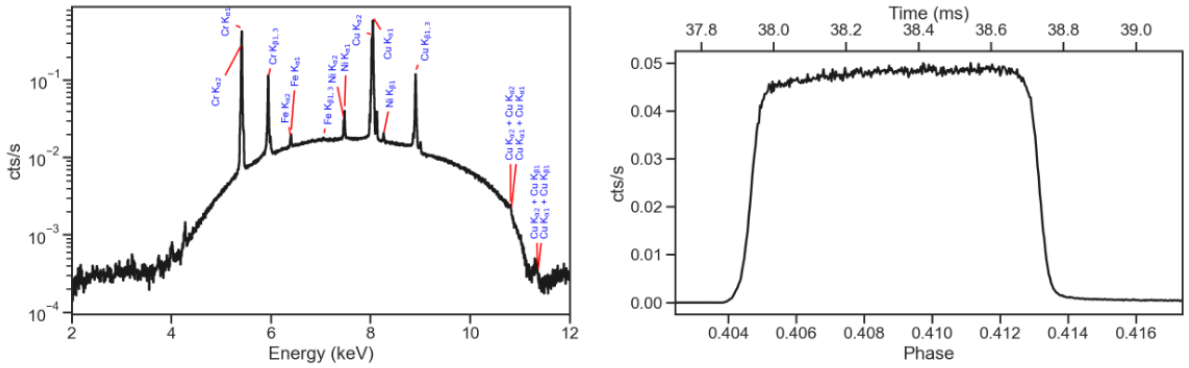

(a) X-ray spectrum (b) Folded light curve

Figure 8: (a) X-ray spectrum and (b) folded light curve using a data set during TC6. Cleaned events of all grades and all pixels except for pixel 12 were combined [13].

In the folded light curve, the timing of the rising edge is known to be affected by the LED current setting, while the falling edge is less affected. We thus derived the falling edges of the events divided into pixels or DERIV_MAX ranges and determined their relative timing. We used the following data set taken with MXS settings of PLS_SPC = 93.75 ms and PLS_LEN = 1 ms.

- 2022/06/09 10:52 - 2022/06/10 01:03 for MXS NOM side
- 2022/06/10 09:56 - 2022/06/11 00:37 for MXS RED side
- 2022/06/12 12:53 - 2022/06/13 00:53 for MXS NOM side
- 2022/06/14 12:54 - 2022/06/15 00:48 for MXS RED side

First, we constrained the C'[H, p] parameters. In order to minimize the DERIV_MAX dependence unknown at this moment, we only used events in the 7.5-8.5 keV range containing the most prominent Cu Ka lines. Figure 9 shows the result. In the top panels, the folded light curves are shown for each pixel. In the bottom panel, the rising and falling edges were detected by calculating the time derivative. Then, the time derivative of each pixel was cross correlated to the reference (pixel 0) to derive the relative offset. The left and right panels respectively show the result before and after the pixel-to-pixel corrections.

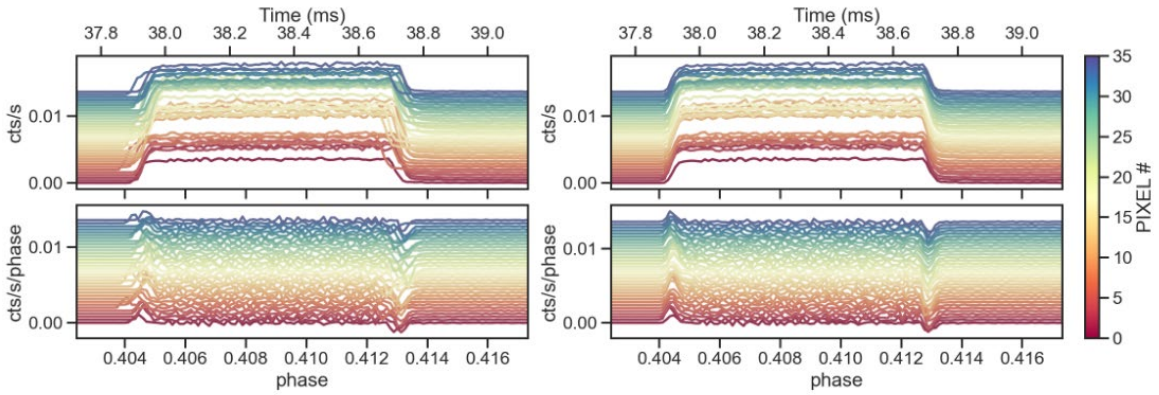

Figure 9 Folded light curves before (left) and after (right) correcting for the pixel-to-pixel timing offset. Different colors are assigned for different pixels[13].

Next, we constrain the B[H] parameter. We combined all pixels after making the pixel-to-pixel correction and divided the events into different DERIV_MAX ranges. Based on the MXS pulse falling edges, the same technic was employed to derive the relative offset (Figure 10). The B[H] parameter was estimated as (-1.1 +/- 0.4) $x10^{-4}$ ms/DERIV_MAX.
The C' parameter for pixel 12 was set as the mean of the remaining 35 pixels as there is no MXS data for the pixel.

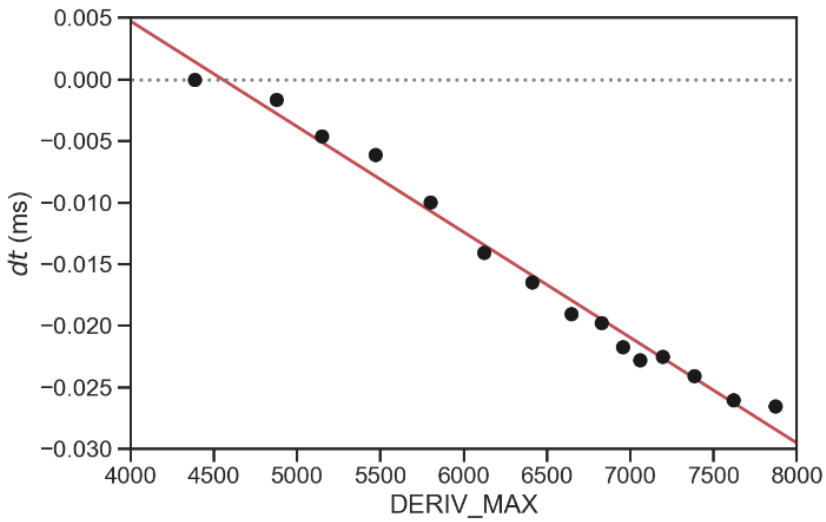

Figure 10 Relative timing offset as a function of DERIV MAX using the Hp events of all pixels except for 12. The linear regression is shown with the red line [13].

The B[H] and C'[H, p] parameters thus derived were applied to the following independent data set obtained with PLS_SPC = 140.625 ms and PLS_LEN = 1 ms.

- 2022/06/13 03:36 - 2022/06/13 06:34 for MXS NOM side
- 2022/06/13 11:37 - 2022/06/13 23:03 for MXS RED side

The resultant offset is shown in Figure 11. We estimate the uncertainty of the correction by using the pixel-to-pixel variation after the correction, which is -4 us in the mean and 5 us in the standard deviation, which are well within the requirement.

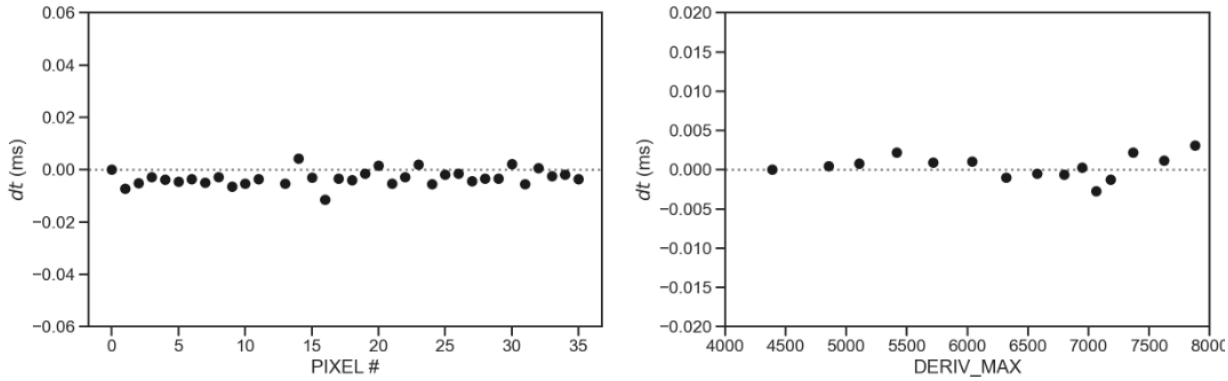

(a) Pixel dependence (b) DERIV_MAX dependence

Figure 11 Relative timing offset as a function of pixel or DERIV MAX using the Hp grade events of all pixels except for 12 in the independent data set [13].

Analysis (2) B[M] and C'[M, p]

In most count rate ranges, the grade branching ratio is dominated by Hp (low count rate regime) or Ls (high count rate regime). Collection of M-res grade events is inefficient unless the count rate is fine-tuned. For the mid-res calibration purposes, therefore, we ran PSP in the forced mid-res mode with the MXS illumination in the low count rate regime, in which all the Hp grade events are processed using the mid-res templates. This data collection was performed with PLS_SPC=93.75 ms and PLS_LEN = 1 ms at

- 2022/07/26 18:30 - 2022/07/27 09:30 for MXS NOM side
- 2022/07/27 20:50 - 2022/07/28 09:40 for MXS RED side

For these data sets, we analyzed in the same way as Analysis (1) and derived B[M] and C'[M, p] parameters. Here, the origin of C'[M, p] remains unambiguous as the forced mid-res option does not yield any Hp data.

First, we constructed light curves folded by the MXS pulse period. We merged the NOM and RED data for the sake of statistics after correcting for their timing offset stemming from the usage of the MXS. Figure 12 shows the result, based on which we derived the pixel-to-pixel parameters relative to pixel 0: i.e., C'[M, p]−C'[M, 0]. We found that C'[M, p]−C'[M, 0] thus derived are consistent with C'[H, p]−C'[H, 0] within errors (Figure 21), thus we decided that C'[M,p] = C'[H, p].

Next, we applied the pixel-to-pixel corrections and divided the events by different DERIV_MAX ranges. The timing offset in the folded light curve is shown in Figure 13, from which we derived the B[M] parameter to be (-1.23 +/− 0.06) x 10^{-4} ms/DERIV_MAX. This is consistent with B[H] in Analysis 1 , so we decided that B[M] ＝B[H].

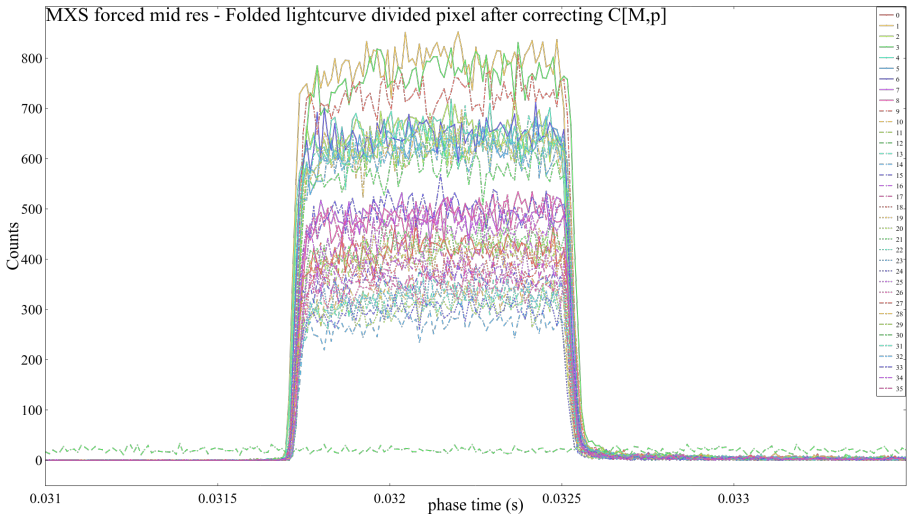

Figure 12 Folded light curve for different pixels using the forced mid-res MXS data combining both NOM and RED sides.

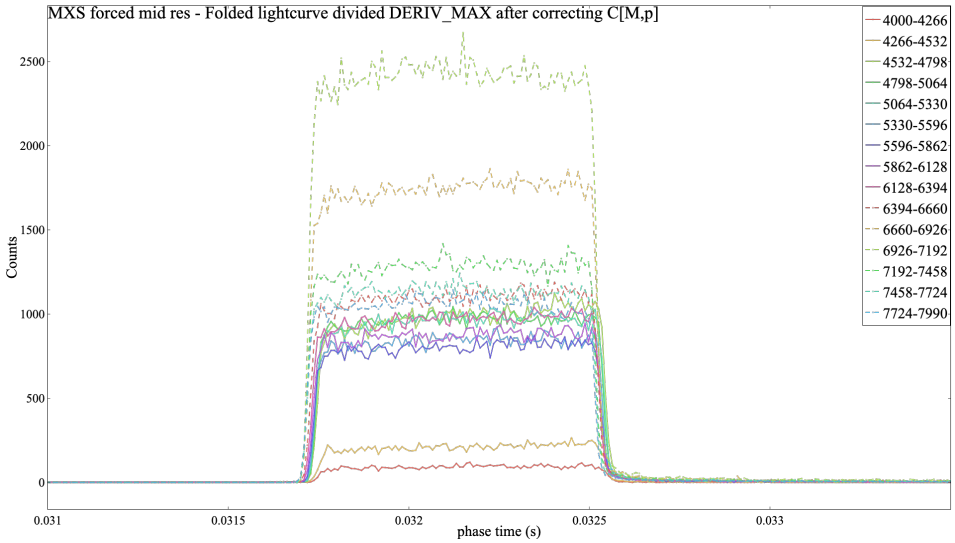

Figure 13 Folded light curve for different DERIV_MAX ranges using the forced mid-res MXS data combining both NOM and RED sides after making pixel-to-pixel corrections.

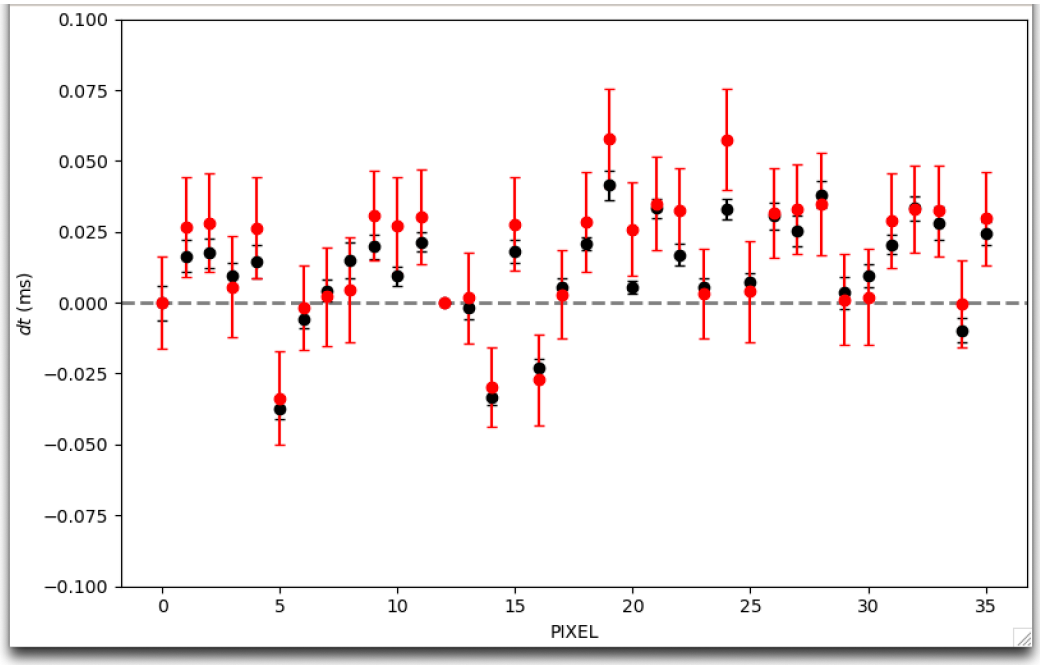

Figure 21 Timing offset among pixels relative to pixel 0 for H-res (black) and M-res (red) events.

Analysis (3) Relative timing among grades C'[H, 0] vs C'[M, 0] vs C'[L, 0]

In order to derive relative timing among different grades: i.e., C'[H, 0] vs C'[M, 0] vs C'[L, 0], we used yet another data set of MXS. The MXS is used in the low count rate regime, in which Hp events dominate. However, there is one exception during the ground testing, in which the MXS was operated in the high count rate regime to accelerate aging before the launch, so that the decay is more stable after the launch. The aging was done only for the nominal side MXS1 twice during the thermal-vacuum test with PLS_SPC = 31.25 ms and PLS_LEN = 15.875 ms at

- 2022/08/10 13:23 – 2022/08/10 23:38 for MXS NOM side
- 2022/08/11 06:52 – 2022/08/11 15:31 for MXS NOM side

Because of the operation, we could obtain events with a more uniform distribution over different grades than any other data sets. Figure 14 shows the folded light curve for each grade, in which timing offset among different grades are evident.

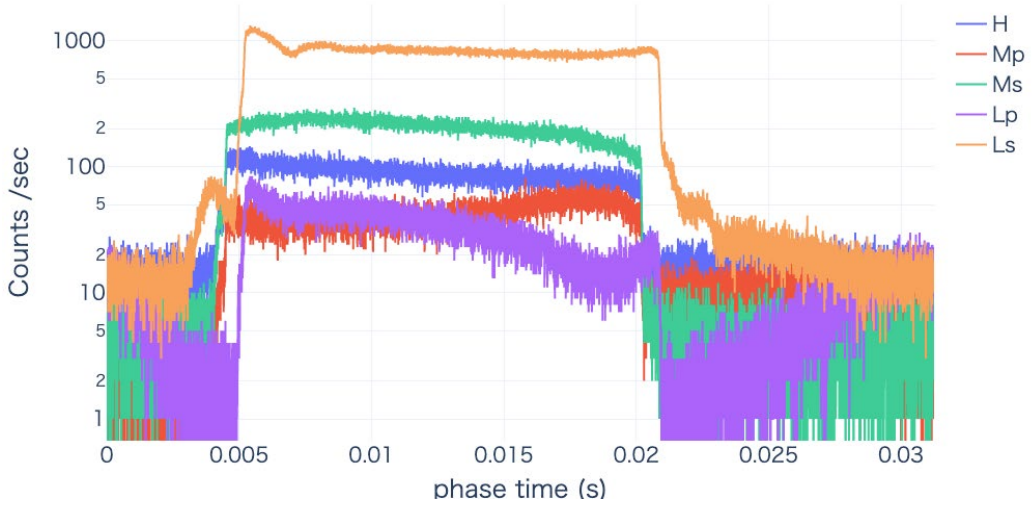

Figure 14 Folded light curve for different grades using the MXS1 aging data for different grades in different colors.

Among the pixels illuminated by MXS1, the pixel 4 had the most uniform event distribution over the grades. We thus measured C'[M, 4] – C'[H, 4] = 0.00 +/- 0.02 ms and C'[L, 4] – C'[H, 4] = 0.72 +/- 0.01 ms.

Analysis (4) B[L] and C'[L, p]

For L-res events, the event time is defined as the sample of the maximum value of the **derivative** of the **adcSample**. The **adcSample** (Figure 15) is the digitized microcalorimeter output from the XBOX sampled at 12.5 kHz, while the **derivative** (Figure 16) is derived by the convolution of the **adcSample** and a boxcar kernel defined as -1/4 for the preceding 8 samples and 1/4 for the current and following 7 samples. The 1/4 is for the normalization. The **adcSample** has 14 bits while **derivative** has 16 bits. Events are triggered when the derivative exceeds the threshold (set at 75 throughout the ground test after 2022 January).

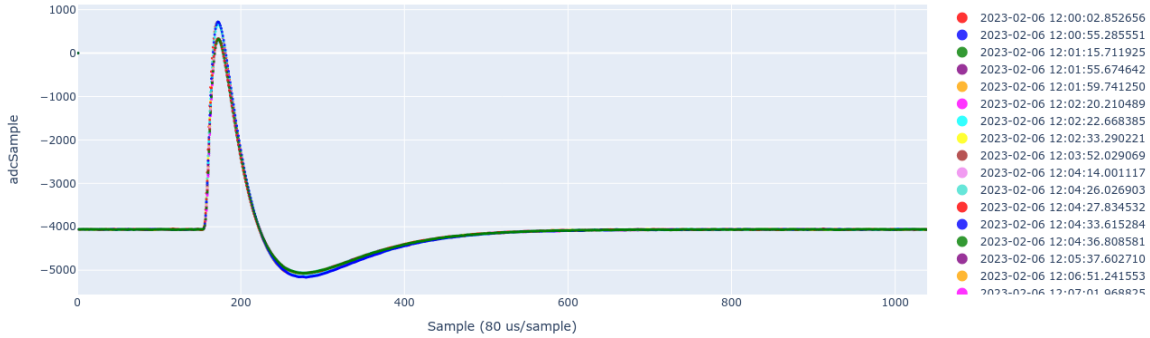

*Figure 15 Examples of **adcSample**.*

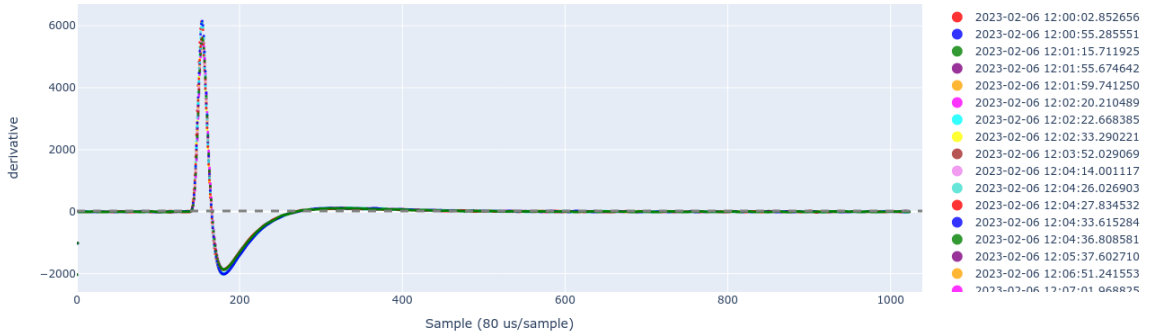

*Figure 16 Examples of **derivative**.*

The time-series data of some randomly selected events are downloaded to the ground, which is called pulse records. We can accumulate sufficient number of pulse records of the clean Hp events and derive the pulse arrival time if the events were graded as L-res. We can thus calculate the offset between H-res and L-res timing. For the H-res and L-res arrival times, we used

time_H = First sample exceeding the threshold (75) + (TRIG_LP – EDB_TRIG_LP) + (TIME_VERNIER)/16
time_L = argmax(**derivative[sample]**)

Here, (TRIG_LP - EDB_TRIG_LP) and (TIME_VERNIER)/16 are the correction for the template shifts respectively in an integer sample and in a sub-sample of a 1/16 sample resolution.

The relative timing (timeL-timeH) was derived for each pixel. Figure 17 shows an example. The relative timing remains stable over DERIV_MAX, which indicates that the DERIV_MAX-dependent correction is unnecessary relative to H, thus B[L] = B[H]. The offset C'[L, p]-C'[H, p] is derived for each pixel as shown in Figure 18. We found that the offset is consistent among all the pixels of 0.80 +/- 0.037 ms (10.01 +/- 0.46 samples). This is also consistent with the result of Analysis (3) using the MXS aging data with a 10% systematics. We adopt the value in Analysis (3) based on actually observed grades. We thus decided to make the offset common among all pixels and derived C'[L, p] by adding the offset to C'[H, p] derived in Analysis (1).

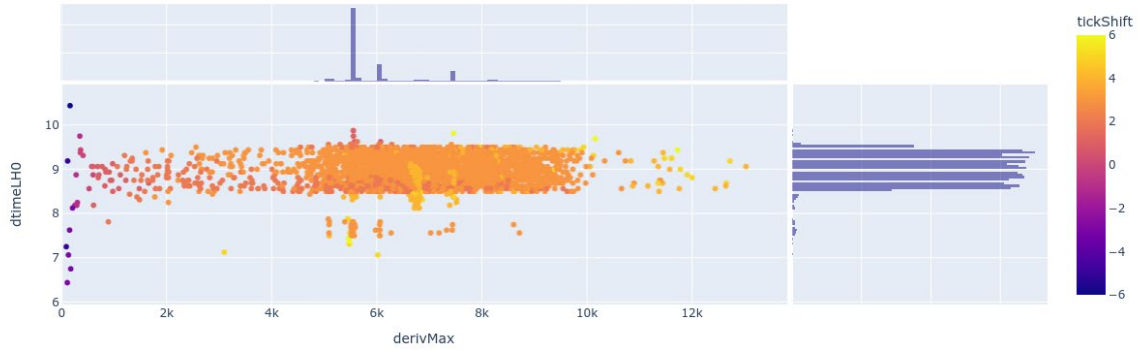

Figure 17 Relative timing offset (in samples) between L-res and H-res arrival times of the same pulse records over DERIV_MAX of the pixel 0 in a TC9 data set.

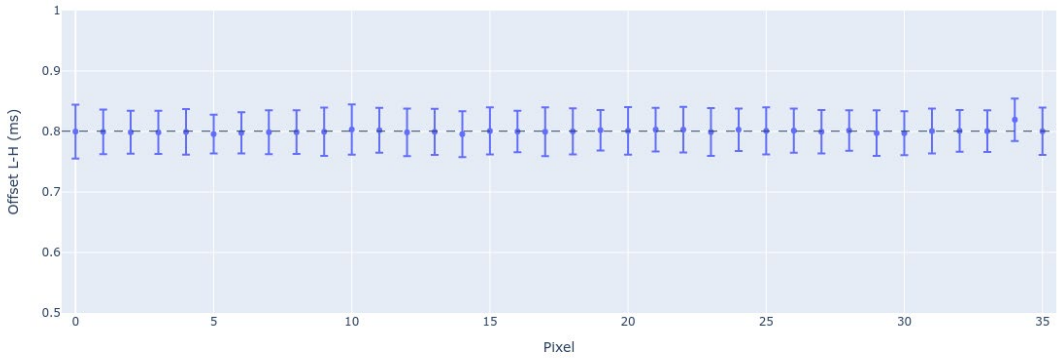

Figure 18 Relative timing between L-res and H-res arrival time of the same pulse record. The error bar indicates the standard deviation from the mean.

Analysis (5) D

The absolute timing (D) is the overall delay of the PSP onboard trigger time with respect to the expected photon arrival time. This offset was calibrated using MXS illumination data sets taken in the Thermal Vac test (Resolve TC7). Since the time of LED on, pulse spacing, and pulse length are all recorded in the FWE HK (the HK_SXS_FWE extension in the Resolve HK1), the MXS phases corresponding to the commanded start and stop can be determined. The actual start and stop of X-ray illumination are delayed due to several factors reflecting the design and performance of the FWE and MXS. These factors include:

- The FWE HK delay of 15.625 ms = 1 SpW time tick, originating from the different handling of the SpW timing signals between the FWE and others such as the PSP.
- The FWE DAC delay of 4 micro-s (for the nominal SpW port of the FWE).
- The FWE pulse phase delay due to the internal time counter for each LED not being reset properly after previous LED off, which has a length of integer multiples of the SpW tick but always less than the pulse spacing. Only appears in the ground test data as a workaround to avoid this delay has been implemented in the FWE/MXS operation.
- The MXS pulse start offset due to the design of the FWE driver circuit, whose length depends on the LED current. The pulse stop offset is negligible and assumed to be zero.

The pulse start delay mentioned above has a strong dependence on the LED current and can be as large as ~0.5 ms for an LED current below 1 mA. To avoid the uncertainty on this delay contributing to the systematic error on the absolute timing, we used the pulse stop timing instead. In determining the pulse fall timing, we employed a BOXCAR derivative to detect the pulse rising and falling edges. The MXS pulse start and stop phases derived with this method essentially give the timings at which the MXS count rate crosses the half of the pulse peak. This means that we also need to take into account the infinite pulse rise/fall (half) times.

The pulse rise/fall time has a small dependence on the LED current, as reported in the MXS pulse parameters CALDB report [10]. Thus, to determine the absolute timing offset, multiple MXS illumination data sets with different LED current settings are needed. The data sets used include both the LED1 and LED3 cases as the pulse rise/fall times were found to be common to both units.

Each MXS illumination data set was processed as follows. First, the relative timing calibration described above was applied to correct for the energy (DERIV_MAX) dependence, grade difference, and pixel variation. Next, MXS phase was assigned after correcting the FWE delays. Then, the MXS pulse-period folded profile was made after applying the standard event screening as used for the relative timing calibration and some additional screenings involving the relations between RISE_TIME, DERIV_MAX, and X-ray energy (EPI), to remove triggered electrical crosstalk children. Here, all the pixels except the cal-pixel were used and the entire

Resolve energy band of 0.3-12 keV were included, although events below 2 keV were statistically poor due to the attenuation at the gate valve. Then, the BOXCAR derivative was calculated for each profile and the observed pulse start and stop times were determined to be the maximum and minimum of the derivative, respectively. Some example profiles of LED3 are shown in Figure 19.

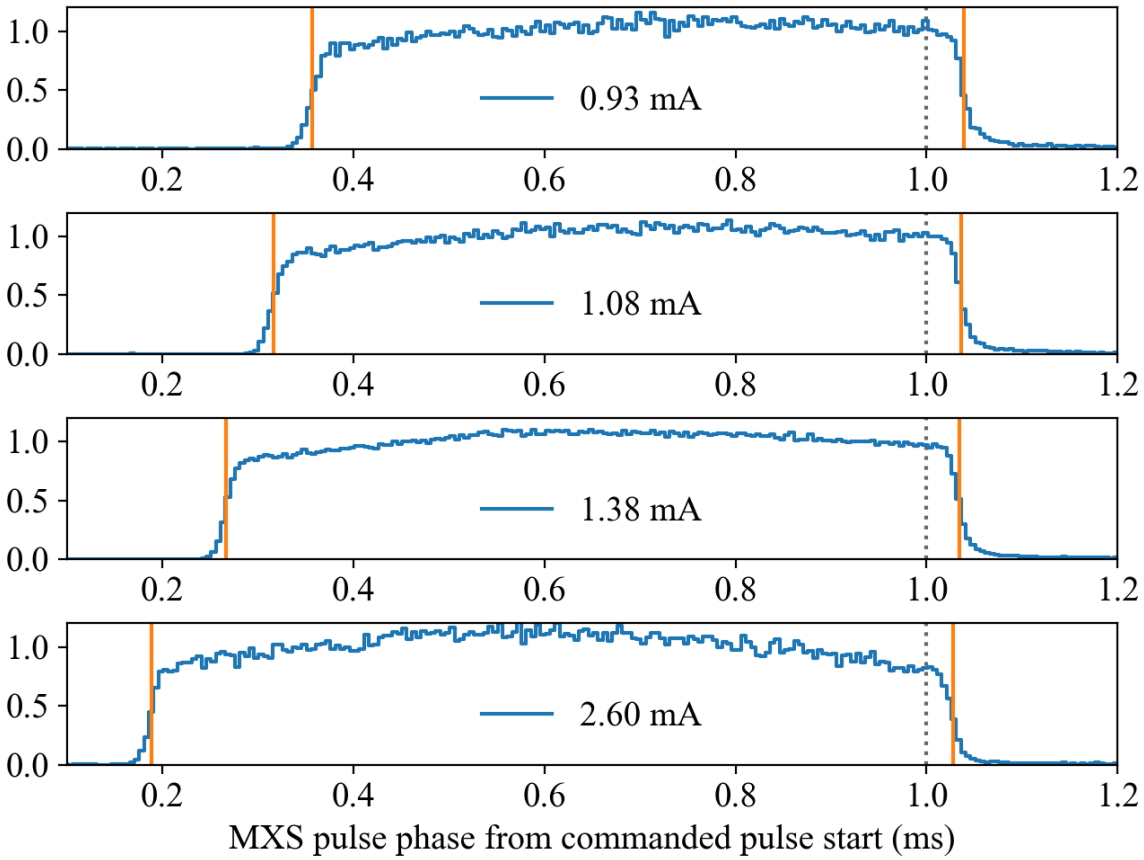

Figure 19. Example MXS pulse profiles. The orange bars on the left and right are the pulse rising and falling edges, respectively, determined with the BOXCAR derivative analysis. The dotted line shows the commanded pulse stop timing. The offset from the falling edge from the commanded pulse stop consists of the pulse fall half time and the PSP absolute timing offset.

The offset of thus-evaluated pulse stop time from the commanded pulse stop is due mainly to the PSP's absolute timing offset, but also contributed by the pulse fall half time depending on the LED current. Figure 20 shows the measured pulse stop offsets for various LED current settings. The LED current dependence was modeled as a power-law function, as done in [10], and the PSP's absolute timing offset was found as the limit of the high LED current, at which the pulse fall half time is negligible. The offset was derived to be D = +284.0 ± 21.5 micro-s. The relatively large statistical uncertainty reflects that of the extrapolated model curve in a very high LED current region of >5 mA where we have no measurements.

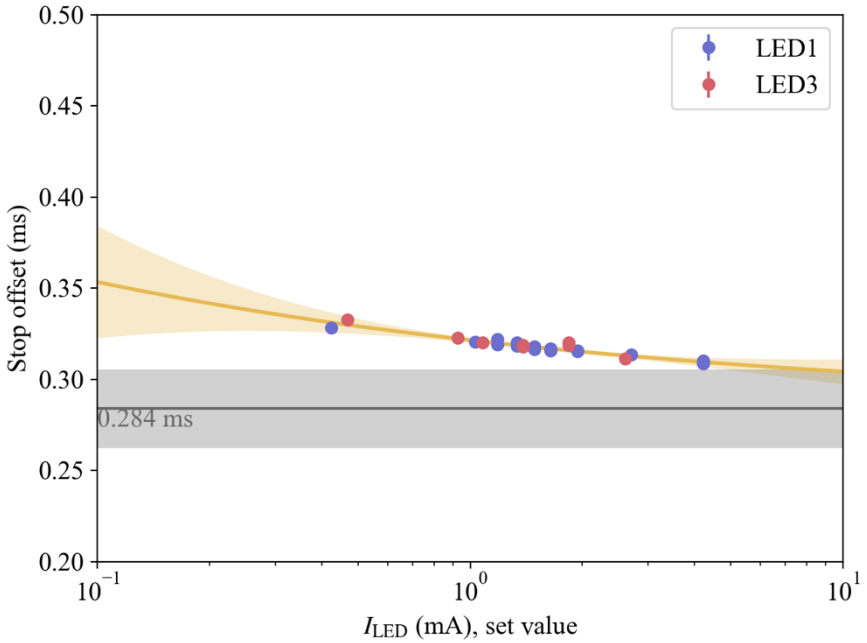

Figure 20. The observed pulse stop offsets fitted as a function of the LED current, consisting a power-law explaining the pulse fall half time and a constant for the PSP absolute timing offset. The total model is shown with gold, while the constant part is shown with gray.

Finally, we compare the derived absolute timing offset with the one for the Hitomi/SXS (Figure 21). The equivalent of d is –83 micro-s, which is the CALDB value of +417 micro-s corrected for the 500 micro-s error due to the inappropriate timing-related header keyword values (TIMEPIXR and TIMEDEL) in the timing calibration of the Hitomi/SXS. Using the *b* coefficients, the offsets at Mn Kα where the template for the optimal filter is made are ~ +237 micro-s for Resolve and ~ –134 micro-s for Hitomi/SXS, resulting in a systematic difference of ~370 micro-s or 4.6 sample. Most of this offset can be attributed to a shift in time added to the template for Resolve to avoid TICK_SHIFT being maxed out at its negative side for low-energy events. As a result, the mean TICK_SHIFT for Mn Kα events is ~3 for Resolve, while it was ~ –0.5 for Hitomi/SXS, explaining 3.5 sample, more than 2/3 of the total 4.6 sample difference. At this moment, there is no conclusive explanation for the remaining ~90 micro-s or ~1.1 sample discrepancy and therefore this should be regarded as a possible systematic uncertainty in the current instrument-level absolute timing, while not necessarily the entire discrepancy needs to be attributed to the calibration error of Resolve. Note that, even after adding other uncertainties such as the statistical error in the absolute offset analysis (~20 micro-s) and imperfectness in the relative timing (up to ~10 micro-s), there is a plenty margin compared to the timing error allocation to the Resolve instrument system (500 micro-s out of the mission end-to-end requirement of 1 ms). Confirmation and further investigation of the discrepancy may be performed after obtaining the in-flight timing calibration data.

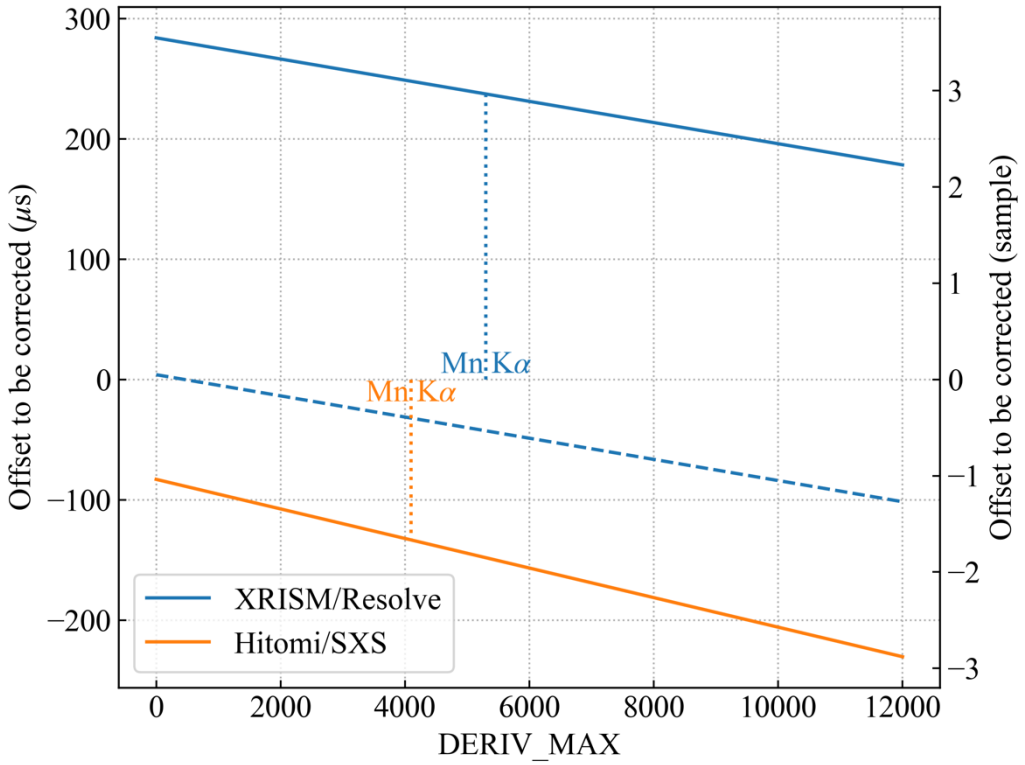

Figure 21. A comparison of the timing offsets between XRISM/Resolve (blue) and Hitomi/SXS (orange). The dashed line for Resolve is the one expected if the template shift of ~3.5 sample was not applied.

Data Analysis: DELTIMES

In this release, we only update the anti-co related parameters: **ANT_SHIFT, ANT_FOL, ANT_PRE**. We applied the A, B, and C (including both C' and D) corrections to all pixel events and selected a pixel event closest in time with the anti-co events over the TC5, 6, 7, and 9 data sets. For the anti-co events, we selected DURATION >= 2 and PHA >= 71 to exclude hardest-end X-ray photons during MXS illumination. We present below the result of events from the anti-co A channel, which is consistent with that for B channel events.

Figure 22 shows the relative timing between anti-co and pixel events for each pixel. They are aligned among all pixels, indicating that pixel-dependent corrections are properly made. Also, pixel 17 and 35 exhibit a wider distribution as they contain electrical cross talk events between anti-co A-side (B-side) readout and pixel 17 (35).

Figure 23 shows the relative timing when all pixels are combined. From the figure, we derived the ANT_SHIFT = –0.157 ms (–1.96 sample). We leave ANT_PRE = ANT_FOL = 0.5 ms (6.25 sample) as used for Hitomi/SXS, which may be optimized later with the in-flight data.

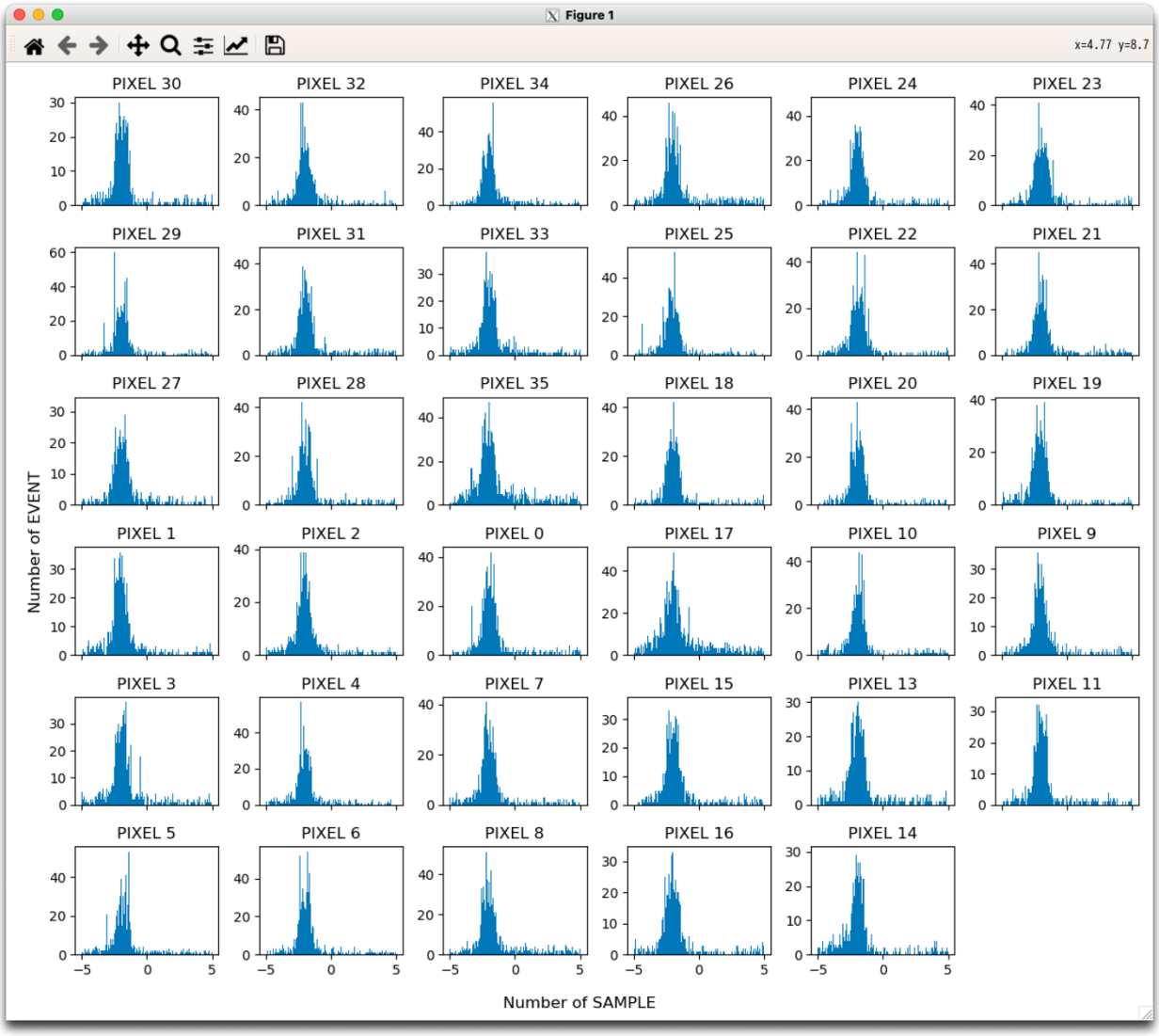

Figure 22 Relative timing between anti-co and pixel events for each pixel.

Here, we briefly revisit the absolute timing difference from Hitomi/SXS by cross-checking it with the ANTSHIFT values. The value for Hitomi/SXS was –610 micro-s, but again, due to the error in the TIMEPIXR and TIMEDEL header keyword values used in the Hitomi calibration, this shift was actually –110 micro-s. The Resolve value of –157 micro-s is within one sample (80 micro-s), which is a similar (slightly better) level of agreement as seen for D.

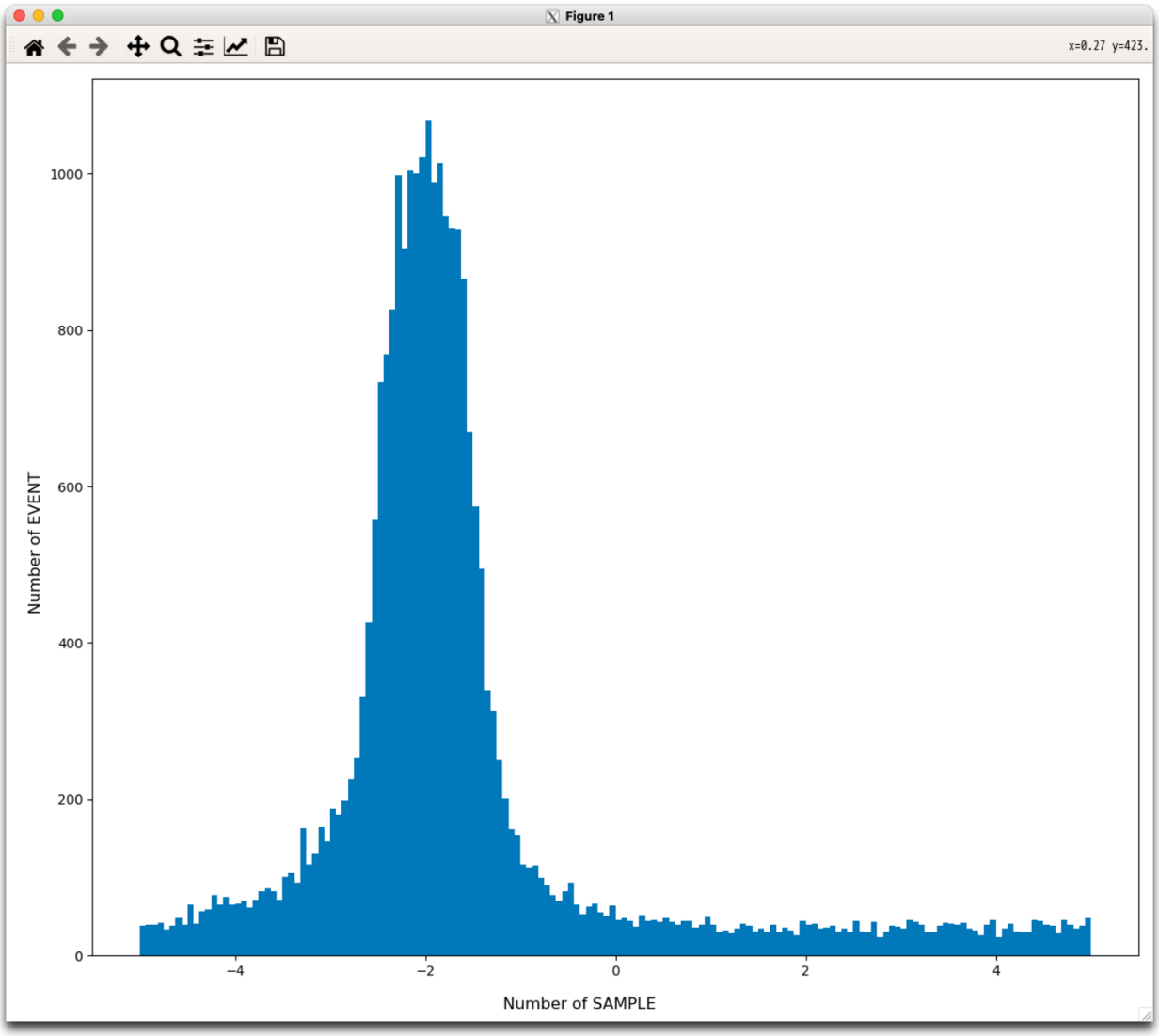

Figure 23 Relative timing between anti-co and pixel events for all pixels combined.

5 References

[1] Leutenegger, M. A., Audard, M., Boyce, K. R., et al., *In-flight verification of the calibration and performance of the ASTRO-H (Hitomi) Soft X-ray Spectrometer*, 2018, Journal of Astronomical Telescopes, Instruments, and Systems, 4, 021407.

[2] Ishisaki, Y., Yamada, S., Seta, H., et al., *In-flight performance of pulse-processing system of the ASTRO-H/Hitomi soft x-ray spectrometer*, 2018, Journal of Astronomical Telescopes,

Instruments, and Systems, 4, 011217.

[3] Terada, Y., et al., *XRISM Time Definition and Assignment*, Version xx.
(To be added once made available)

[4] Eckart, M.E. and the Resolve Instrument Team, *Log of Resolve Detector Thresholds and Optimal Filter Templates calibration report* (RESOLVE-SCI-RPT-0058, XRISM-RESOLVE-CALDB-CONFTHRE-217).

[5] Kilbourne, C. A., Sawada, M., Tsujimoto, M., et al., *In-flight calibration of Hitomi Soft X-ray Spectrometer. (1) Background*, 2018, Publication of Astronomical Society of Japan, 70, 18.

[6] Tashiro, M., Koyama, S., Kilbourne, K., et al., *ASTRO-H Instrument Calibration Report SXS timing coefficients*, Version 2.1 (August 29, 2016).
https://heasarc.gsfc.nasa.gov/docs/hitomi/calib/caldb_doc/asth_sxs_caldb_coeftime_v20160829.pdf

[7] Hitomi Collaboration, et al., *Hitomi X-ray studies of giant radio pulses from the Crab pulsar*, 2018, Publication of Astronomical Society of Japan, 70, 15.

[8] Molkov, S., Jourdain, E., Roques, J. P., *Absolute Timing of the Crab Pulsar with the INTEGRAL/SPI Telescope*, 2010, The Astrophysical Journal, 708, 403.

[9] Sawada, M., Koyama, S., Kilbourne, C., et al., *Timing calibration of Resolve microcalorimeter spectrometer on XRISM*, 2019, 14th IACHEC meeting.
http://iachec.scripts.mit.edu/meetings/2019/presentations/WGII_sawada.pdf

[10] Cumbee, R., M. Sawada, de Vries, C., et al., *The Resolve Modulated X-ray Source Pulse Parameters calibration report* (RESOLVE-SCI-RPT-0054, XRISM-RESOLVE-CALDB-MXSPARAMS-218).

[11] Shimoda, Y., Seta, H., Tashiro, M. S., et al., *Development of a Digital Signal Processing System for the X-Ray Microcalorimeter Onboard ASTRO-H (II)*, Journal of Low Temperature Physics, 2012, 167, 575.

[12] Ishisaki, Y. et al., *Status of resolve instrument onboard x-ray imaging and spectroscopy mission (XRISM)*, Proc. SPIE 12181, Space Telescopes and Instrumentation 2022: Ultraviolet to Gamma Ray, 121811S (31 August 2022); doi: 10.1117/12.2630654

[13] Omama, T., Tsujimoto, M., Sawada, M., et al., *Relative timing calibration of the Resolve x-ray microcalorimeter onboard XRISM using the modulated x-ray source*, Proc. SPIE,12181, Space Telescopes and Instrumentation 2022: Ultraviolet to Gamma Ray, 1218162 (31 August

2022); doi: 10.1117/12.2629753